Dalton Transactions

Accepted Manuscript

ROYAL SOCIETY OF CHEMISTRY

www.rsc.org/dalton

Cite this: DOI: 10.1039/c0xx00000x

www.rsc.org/xxxxxx

ARTICLE TYPE

Syntheses, structures and electrochemical properties of a class of 1-D double chain polyoxotungstate hybrids $[H_2dap][Cu(dap)_2]_{0.5}[Cu(dap)_2(H_2O)][Ln(H_2O)_3(\alpha\text{-}GeW_{11}O_{39})]\cdot 3H_2O$

Jun-Wei Zhao,*[a,b] Yan-Zhou Li,[a] Fan Ji,[a] Jing Yuan,[a] Li-Juan Chen,[a] and Guo-Yu Yang*[,b]

Received (in XXX, XXX) Xth XXXXXXXXX 20XX, Accepted Xth XXXXXXXXX 20XX
DOI: 10.1039/b000000x

A series of novel organic–inorganic hybrid 1-D double chain germanotungstates $[H_2dap][Cu(dap)_2]_{0.5}[Cu(dap)_2(H_2O)][Ln(H_2O)_3(\alpha\text{-}GeW_{11}O_{39})]\cdot 3H_2O$ [Ln = La^{III} (**1**), Pr^{III} (**2**), Nd^{III} (**3**), Sm^{III} (**4**), Eu^{III} (**5**), Tb^{III} (**6**), Er^{III} (**7**)] (dap = 1,2-diaminopropane) have been hydrothermally prepared and structurally characterized by elemental analyses, powder X-ray diffraction (PXRD), IR spectra, thermogravimetric (TG) analyses, X-ray photoelectron spectroscopy (XPS) and single-crystal X-ray diffraction. The most prominent structural feature of **1–7** is that the $[Ln(H_2O)_3(\alpha\text{-}GeW_{11}O_{39})]^{5-}$ moieties are firstly connected with each other via the W–O–Ln–O–W bridges creating a 1-D $\{[Cu(dap)_2(H_2O)][Ln(H_2O)_3(\alpha\text{-}GeW_{11}O_{39})]\}_n^{3n-}$ polymeric chain and then two adjacent antiparallel 1-D polymeric chains are linked together through $[Cu(dap)_2]^{2+}$ linkages giving rise to the rare organic–inorganic hybrid 1-D Cu^{II}–Ln^{III} heterometallic double-chain architectures. To the best of our knowledge, **1–7** represent the first 1-D double-chain Cu^{II}–Ln^{III} heterometallic germanotungstates. The variable-temperature magnetic susceptibilities of **2**, **4** and **7** have been investigated. Furthermore, the solid-state electrochemical and electro-catalytic properties of **3** and **4** have been carried out in 0.5 mol·L^{-1} Na_2SO_4 + H_2SO_4 aqueous solution by entrapping them in a carbon paste electrode. **3** and **4** display apparent electro-catalytic activities for the nitrite, bromate and hydrogen peroxide reduction.

Introduction

Polyoxometalates (POMs) are polynuclear metal–oxo complexes with unique physical and chemical performances. The oxygen-rich surface of defect or lacunary POMs renders them become excellent inorganic multidentate candidates to integrate oxophilic d- or f-block metals, giving rise to a variety of novel d- or f-block metal substituted POMs with possible applications spanning a range of domains such as materials science, electro-catalysis and magnetism.[1]

In the past decades, various lacunary POMs have been used to capture transition-metal (TM) cations to form novel complexes with interesting structures and properties. Among the family of POMs, TM-substituted polyoxotungstates (POTs) are ideal models for researching magnetic exchange interactions within TM centers. Thus, predominant interest is driven by various electronic and magnetic properties of TM-substituted POTs, to date, so numerous TM-substituted POTs were found,[2] such as $[H_{56}Fe_{28}P_8W_{48}O_{248}]^{28-}$,[2a] $[Cu_{20}Cl(OH)_{24}(H_2O)_{12}(P_8W_{48}O_{184})]^{25-}$,[2b] $[Nb_4O_6(Nb_3SiW_9O_{40})_4]^{20-}$,[2c] $[(P_2W_{15}Ti_3O_{62})_4\{Ti(OH)_3\}_4Cl]^{45-}$,[2d] $[Ni(enMe)_2]_3[H_6Ni_{20}P_4W_{34}(OH)_4O_{136}(enMe)_8(H_2O)_6]\cdot 12H_2O$,[2e] $[Ni(en)_2(H_2O)]_2[H_8Ni_{20}P_4W_{34}(OH)_4O_{136}(en)_9(H_2O)_4]\cdot 16H_2O$,[2e] $[Mn_{19}(OH)_{12}(SiW_{10}O_{37})_6]^{34-}$,[2f] and $[(Mn^{II}(H_2O)_3)_2(K\subset\{\alpha\text{-}GeW_{10}Mn^{II}{}_2O_{38}\}_3)]^{19-}$.[2g] Compared with TM cations, though the larger sizes of lanthanide (Ln) cations prevent them from fully incorporation to lacunary POT matrixes, their oxophilicity and high coordination numbers provide available conditions for further deriving complicate structures. Moreover, their functionality such as luminescence, magnetism or Lewis acid catalysis can be also delivered to the desired outcomes during the course of derivatization or functionality.[3] Therefore, in recent years, a large number of Ln-containing POTs have been obtained.[4] For instance, in 1997, Pope and co-workers reported a Ce_{16}-containing huge POT $[As_{12}Ce_{16}W_{148}O_{524}(H_2O)_{36}]^{76-}$.[4a] In 2001, an europium containing tetrameric phosphotungstate $[(PEuW_{10}O_{38})_4(W_3O_{14})]^{30-}$ was discovered by Francesconi's group.[4b] In 2002, Gouzerh et al. described two cerium-containing POTs $[Ce(H_2O)_5As_4W_{40}O_{140}]^{25-}$ and $[(SbW_9O_{33})_4\{WO_2(H_2O)\}_2Ce_3(H_2O)_8(Sb_4O_4)]^{19-}$.[4c] In 2003, two crown-shaped europium containing arsenotungstates $[K\subset\{Eu(H_2O)_2(\alpha\text{-}AsW_9O_{33})\}_6]^{35-}$ and $[Cs\subset\{Eu(H_2O)_2(\alpha\text{-}AsW_9O_{33})\}_4]^{23-}$ were seperated.[4d] In 2007, an unprecedented Ce_{20}-containing gigantic germanetungstate (GT) $[Ce_{20}Ge_{10}W_{100}O_{376}(OH)_4(H_2O)_{30}]^{56-}$ was prepared.[4e] Later, the longest Ln substituted POT molecule $[Gd_8As_{12}W_{124}O_{432}(H_2O)_{36}]^{60-}$ was discovered.[4f] With the rapid development of POM chemistry, the first POM-based TM–Ln heterometallic derivative (PBTLHD) was reported in 2004.[5] From then on, the design and synthesis of PBTLHDs have gradually become an emerging research field of POM chemistry owing to their potential applications in magnetism and catalysis as well as their intriguing architectures and topologies.[6] However, as previously reported, there are unavoidable competitive reactions among highly negative POM precursors, strongly oxyphilic Ln cations and less active TM cations in the reaction system, so the simultaneous combinations of lacunary POMs with TM and Ln components are comparatively difficult in the same system,[7] which seems to be the key factor of the small number of reports on PBTLHDs.[8] So,

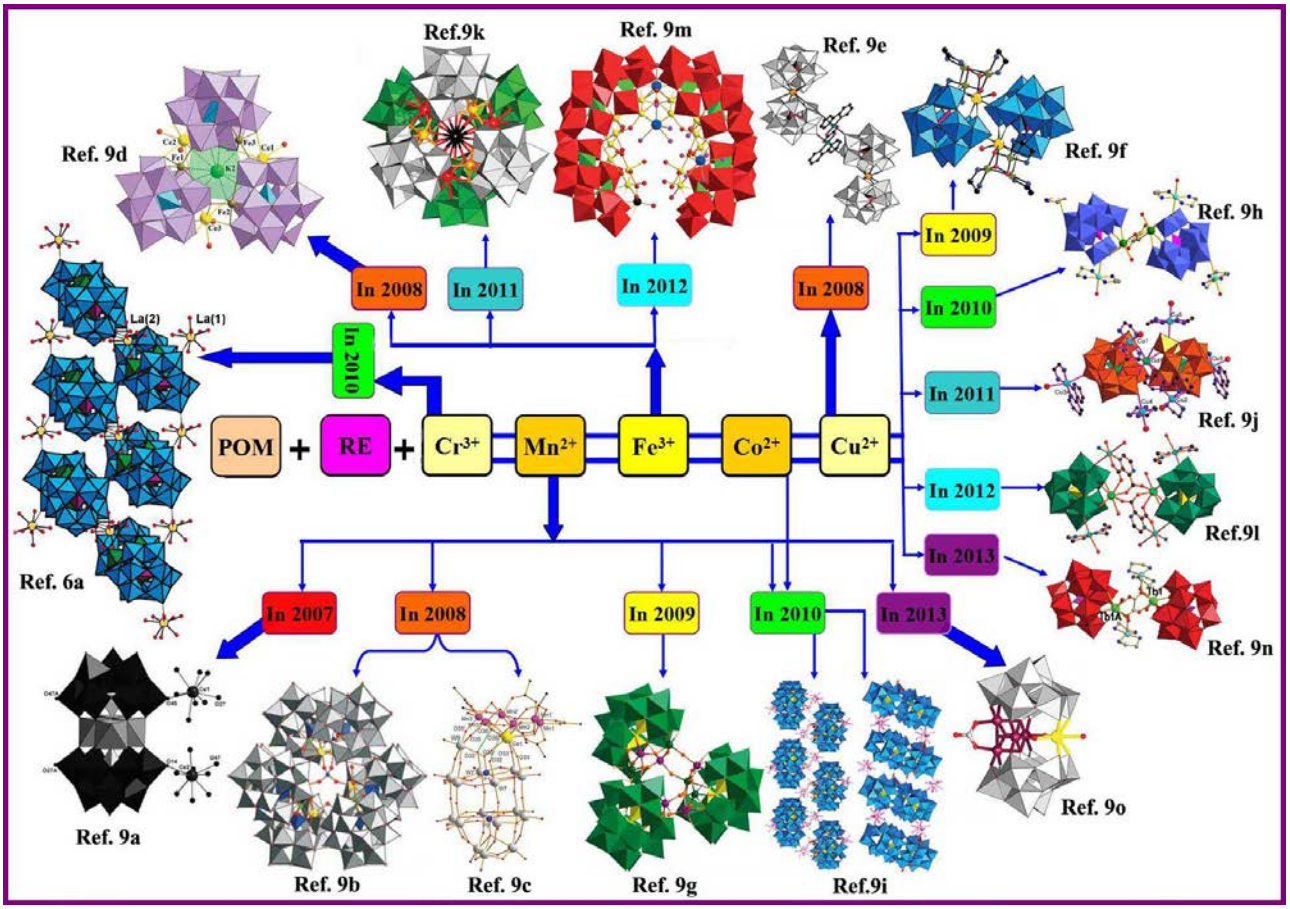

Fig. 1 the summary of some typical 3d–4f POTs.

currently, great efforts have been devoted to exploitation of novel PBTLHDs and some typical species have been successively synthesized (Fig. 1).[9,6a] Among PBTLHDs, only minority of TM–Ln-containing GTs have been reported.[10] For a example, Reinoso et al. prepared two Weakley-type heterometallic Cu/Mn–Ce substituted GTs $[\{Ce^{III}(H_2O)_2\}_2Mn^{III}_2(B\text{-}\alpha\text{-}GeW_9O_{34})_2]^{8-}$,[10a] and $[\{Ce^{IV}(OAc)\}Cu^{II}_3(H_2O)(B\text{-}\alpha\text{-}GeW_9O_{34})_2]^{11-}$[10b] by reactions of Ce^{IV} cations with the synthons $[Mn^{II}_4(H_2O)_2(B\text{-}\alpha\text{-}GeW_9O_{34})_2]^{12-}$ [11] and $[Cu^{II}_4(H_2O)_2(B\text{-}\alpha\text{-}GeW_9O_{34})_2]^{12-}$ [11] in 2010 and 2011, respectively. Furthermore, a giant crown-shaped GT $Na_{40}K_6[Ni(H_2O)_6]_3[K\subset K_7Ce_{24}Ge_{12}W_{120}O_{456}(OH)_{12}(H_2O)_{64}]\cdot 178H_2O$ was also obtained by them.[10c] As a result, the search and exploration on novel TM–Ln-containing GTs are still an incipient field. Under this background, we began to explore this challengeable area. Three organic–inorganic hybrid $\{Cu_3LnO_4\}$ cubane inserted GTs $\{[Cu(en)_2(H_2O)][Cu_3Ln(en)_3(OH)_3(H_2O)_2](\alpha\text{-}GeW_{11}O_{39})\}_2\cdot nH_2O$ (Ln = Eu^{III}, n = 11; Ln = Tb^{III}, n = 11; Ln = Dy^{III}, n = 10) and three Cu–Ln-containing GT tetramers $Na_2H_6[Cu(en)_2(H_2O)]_8\{Cu(en)_2[La(\alpha\text{-}GeW_{11}O_{39})_2]_2\}\cdot 18H_2O$, $K_4H_2[Cu(en)_2(H_2O)_2]_5[Cu(en)_2(H_2O)]_2[Cu(en)_2]_2\{Cu(en)_2[Pr(\alpha\text{-}GeW_{11}O_{39})_2]_2\}\cdot 16H_2O$ and $KNa_2H_7[enH_2]_3[Cu(en)_2(H_2O)]_2[Cu(en)_2]_2\{Cu(en)_2[Er(\alpha\text{-}GeW_{11}O_{39})_2]_2\}\cdot 15H_2O$ were first synthesized in our laboratory.[12a] Very recently, we separated two unusual 1-D copper–bridged tetrahedral POM nanoclusters with tetrameric rare earth cores and GT vertexes $Na_3H_7[Cu(en)_2]_5[Cu(en)_2(H_2O)]_2[RE_4Ge_4W_{46}O_{164}(H_2O)_3]\cdot nH_2O$ (RE = Gd^{III}, n = 25; RE = Y^{III}, n = 23).[12b] In order to profoundly explore this research domain, we used dap (dap = 1,2-diaminopropane) instead of en, and finally, we made a series of novel organic–inorganic hybrid 1-D double chain GTs $[H_2dap][Cu(dap)_2]_{0.5}[Cu(dap)_2(H_2O)][Ln(H_2O)_3(\alpha\text{-}GeW_{11}O_{39})]\cdot 3H_2O$ [Ln = La^{III} (**1**), Pr^{III} (**2**), Nd^{III} (**3**), Sm^{III} (**4**), Eu^{III} (**5**), Tb^{III} (**6**), Er^{III} (**7**)], which are constituted by two 1-D antiparallel $\{[Cu(dap)_2(H_2O)][Ln(H_2O)_3(\alpha\text{-}GeW_{11}O_{39})]\}_n^{3n-}$ polymeric chains via $[Cu(dap)_2]^{2+}$ bridges. The variable-temperature magnetic susceptibilities of **2**, **4** and **7** have been measured. Furthermore, the solid-state electrochemical and electro-catalytic properties of **3** and **4** have been carried out in 0.5 mol^{-1} $Na_2SO_4 + H_2SO_4$ aqueous solution by entrapping them in a carbon paste electrode (CPE). **3**- and **4**-CPEs were employed to electro-catalyze the reduction of nitrite, bromate and hydrogen peroxide. The results indicate that **3**- and **4**-CPE exhibit obvious electro-catalytic activities towards the reduction of nitrite, bromate and hydrogen peroxide.

Experimental

Materials and physical measurements

All chemicals were commercially purchased and used without further purification. $K_8Na_2[A\text{-}\alpha\text{-}GeW_9O_{34}]\cdot 25H_2O$ was synthesized according to the literature[13] and characterized by IR spectra. Elemental analyses (C, H and N) were performed on a Perkin–Elmer 2400–II CHNS/O analyzer. Inductively coupled plasma atomic emission spectrometry (ICP-AES) was performed on a

Perkin-Elmer Optima 2000 ICP-AES spectrometer. Powder X-ray diffraction (PXRD) spectra were performed on a Bruker D8 ADVANCE instrument with Cu Ka radiation (λ = 1.54056 Å). IR spectra were obtained from solid samples palletized with KBr on a Nicolet 170 SXFT–IR spectrometer in the range 400–4000 cm^{-1}. TGA were performed under a N_2 atmosphere on a Mettler–Toledo TGA/SDTA 851^e instrument with a heating rate of 10 ^oC min^{-1} from 25 to 700 ^oC. XPS spectra were recorded on an Axis Ultra X-ray photoelectron spectrometer and XPS analyses were corrected with reference to C_{1s} (284.6 eV). Magnetic measurements were carried out with a Quantum Design MPMS XL–7 magnetometer in the temperature range of 2–300 K. The magnetic susceptibility data were corrected from the diamagnetic contributions as deduced by using Pascal's constant tables. Cyclic voltammograms were recorded on a CS electrochemical workstation (Wuhan Corrtest Instrument Co. LTD) at room temperature. A conventional three-electrode system was used. Platinum gauze was used as a counter electrode, and an Ag/AgCl electrode was referenced. Chemically bulk- modified carbon paste electrodes (CPEs) were used as working electrodes.

Preparations of 1–7

$[H_2dap][Cu(dap)_2(H_2O)][Cu(dap)_2]_{0.5}[La(H_2O)_3(\alpha\text{-}GeW_{11}O_{39})]\cdot 3H_2O$ (1). A mixture of $K_8Na_2[A\text{-}\alpha\text{-}GeW_9O_{34}]\cdot 25H_2O$ (0.304 g, 0.099 mmol), $CuCl_2\cdot 2H_2O$ (0.083 g, 0.487 mmol), $LaCl_3$ (0.098 g, 0.399 mmol), dap (0.10 mL, 1.201 mmol) and H_2O (5 mL, 278 mmol) was stirred for 2 h, sealed in a 25 mL Teflon-lined steel autoclave, kept at 160 °C for 5 d and then cooled to room temperature. Purple prismatic crystals were obtained by filtering, washed with distilled water and then dried in air at ambient temperature. Yield: *ca*. 30% (based on $K_8Na_2[A\text{-}\alpha\text{-}GeW_9O_{34}]\cdot 25H_2O$). Anal. calcd. (found %) for $C_{12}H_{56}Cu_{1.50}GeN_8O_{46}LaW_{11}$ (**1**): C 4.27 (4.39), H 1.67 (1.82), N 3.32 (3.17), Cu 2.82 (2.72), Ge 2.15 (2.30), La 4.11 (4.32), W 59.87 (59.94). IR (KBr pellets, cm^{-1}): 3461(vs), 3306(w), 3253(w), 3139(w), 2968(w), 2928 (w), 1621(m), 1587(m), 1461(w), 1384(w), 1168(w), 1062(m), 1020 (m), 940(s), 873(vs), 811(vs), 767(vs), 692(s) (Fig. S1A , S1B).

$[H_2dap][Cu(dap)_2(H_2O)][Cu(dap)_2]_{0.5}[Pr(H_2O)_3(\alpha\text{-}GeW_{11}O_{39})]\cdot 3H_2O$ (2). A mixture of $K_8Na_2[A\text{-}\alpha\text{-}GeW_9O_{34}]\cdot 25H_2O$ (0.366 g, 0.119 mmol), $CuCl_2\cdot 2H_2O$ (0.109 g, 0.639 mmol), $PrCl_3$ (0.083 g, 0.336 mmol), dap (0.10 mL, 1.201 mmol) and H_2O (5 mL, 278 mmol) was stirred for 2 h, sealed in a 25 mL Teflon-lined steel autoclave, kept at 160 °C for 5 d and then cooled to room temperature. Purple prismatic crystals were obtained by filtering, washed with distilled water and then dried in air at ambient temperature. Yield: ca. 26% (based on $K_8Na_2[A\text{-}\alpha\text{-}GeW_9O_{34}]\cdot 25H_2O$). Anal. calcd. (found %) for $C_{12}H_{56}Cu_{1.50}GeN_8O_{46}PrW_{11}$: C 4.26 (4.37), H 1.67 (1.77), N 3.32 (3.44), Cu 2.82 (2.95), Ge 2.15 (2.03), Pr 4.17 (4.04), W 59.83 (59.96). IR (KBr pellets, cm^{-1}): 3465(vs), 3307(w), 3248(w), 3142(w), 2969(w), 2928(w), 1617(m), 1589(m), 1468(w), 1386(w), 1167(w), 1056(m), 1023 (m), 940(s), 876(vs), 813(vs), 764(vs), 687(s), (Fig. S1A, S1B).

$[H_2dap][Cu(dap)_2(H_2O)][Cu(dap)_2]_{0.5}[Nd(H_2O)_3(\alpha\text{-}GeW_{11}O_{39})]\cdot 3H_2O$ (3). A mixture of $K_8Na_2[A\text{-}\alpha\text{-}GeW_9O_{34}]\cdot 25H_2O$ (0.362 g, 0.118 mmol), $CuCl_2\cdot 2H_2O$ (0.088 g, 0.516 mmol), $NdCl_3$ (0.095 g, 0.379 mmol), dap (0.10 mL, 1.201 mmol) and H_2O (5 mL, 278 mmol) was stirred for 2 h, sealed in a 25 mL Teflon-lined steel autoclave, kept at 160 °C for 5 d and then cooled to room temperature. Purple prismatic crystals were obtained by filtering, washed with distilled water and then dried in air at ambient temperature. Yield: ca. 32% (based on $K_8Na_2[A\text{-}\alpha\text{-}GeW_9O_{34}]\cdot 25H_2O$). Anal. calcd. (found %) for $C_{12}H_{56}Cu_{1.50}GeN_8O_{46}NdW_{11}$ (**3**): C 4.26 (4.35), H 1.67 (1.79), N 3.31 (3.20), Cu 2.82 (2.74), Nd 4.26 (4.42), Ge 2.15 (2.09), W 59.78 (59.67). IR (KBr pellets, cm^{-1}): 3470(vs), 3302(w), 3251(w), 3140(w), 2971 (w), 2932 (w), 1619(m), 1588(m), 1462(w), 1397(w), 1168(w), 1064 (m), 1020(m), 941(s), 876(vs), 813(vs), 767(vs), 695(s) (Fig. S1A, S1B).

$[H_2dap][Cu(dap)_2(H_2O)][Cu(dap)_2]_{0.5}[Sm(H_2O)_3(\alpha\text{-}GeW_{11}O_{39})]\cdot 3H_2O$ (4). A mixture of $K_8Na_2[A\text{-}\alpha\text{-}GeW_9O_{34}]\cdot 25H_2O$ (0.308 g, 0. 100 mmol), $CuCl_2\cdot 2H_2O$ (0.086 g, 0.504 mmol), $SmCl_3$ (0.084 g, 0.327 mmol), dap (0.10 mL, 1.201 mmol) and H_2O (5 mL, 278 mmol) was stirred for 2 h, sealed in a 25 mL Teflon-lined steel autoclave, kept at 160 °C for 5 d and then cooled to room temperature. Purple prismatic crystals were obtained by filtering, washed with distilled water and then dried in air at ambient temperature. Yield: ca. 35% (based on $K_8Na_2[A\text{-}\alpha\text{-}GeW_9O_{34}]\cdot 25H_2O$). Anal. calcd. (found %) for $C_{12}H_{56}Cu_{1.50}GeN_8O_{46}SmW_{11}$ (**4**): C 4.25 (4.11), H 1.67 (1.79), N 3.31 (3.18), Cu 2.81 (2.76), Ge 2.14 (2.25), Sm 4.44 (4.35), W 59.67 (59.50). IR (KBr pellets, cm^{-1}): 3468(vs), 3306(w), 3253(w), 3140(w), 2969 (w), 2930(w), 1630(m), 1589(m), 1458(w), 1398(w), 1168(w), 1064(m), 1020(m), 941(s), 876(vs), 814(vs), 769(vs), 695(s) (Fig. S1A, S1B).

$[H_2dap][Cu(dap)_2(H_2O)][Cu(dap)_2]_{0.5}[Eu(H_2O)_3(\alpha\text{-}GeW_{11}O_{39})]\cdot 3H_2O$ (5). A mixture of $K_8Na_2[A\text{-}\alpha\text{-}GeW_9O_{34}]\cdot 25H_2O$ (0.302 g, 0.098 mmol), $CuCl_2\cdot 2H_2O$ (0.098 g, 0.575 mmol), $EuCl_3$ (0.089 g, 0.345 mmol), dap (0.10 mL, 1.201 mmol) and H_2O (5 mL, 278 mmol) was stirred for 2 h, sealed in a 25 mL Teflon-lined steel autoclave, kept at 160 °C for 5 d and then cooled to room temperature. Purple prismatic crystals were obtained by filtering, washed with distilled water and then dried in air at ambient temperature. Yield: ca. 33% (based on $K_8Na_2[A\text{-}\alpha\text{-}GeW_9O_{34}]\cdot 25H_2O$). Anal. calcd. (found %) for $C_{12}H_{56}Cu_{1.50}GeN_8O_{46}EuW_{11}$ (**5**): C 4.25 (4.36), H 1.66 (1.88), N 3.30 (3.17), Cu 2.81 (2.68), Ge 2.14 (2.01), Eu 4.48 (4.66), W 59.64 (59.83). IR (KBr pellets, cm^{-1}): 3467(vs), 3306(w), 3252(w), 3140(w), 2964 (w), 2928 (w), 1620(m), 1588(m), 1461(w), 13917(w), 1175(w), 1065(m), 1020(m), 942(s), 875(vs), 810(vs), 766(vs), 693(s) (Fig. S1A,S1B).

$[H_2dap][Cu(dap)_2(H_2O)][Cu(dap)_2]_{0.5}[Tb(H_2O)_3(\alpha\text{-}GeW_{11}O_{39})]\cdot 3H_2O$ (6). A mixture of $K_8Na_2[A\text{-}\alpha\text{-}GeW_9O_{34}]\cdot 25H_2O$ (0.287 g, 0.093 mmol), $CuCl_2\cdot 2H_2O$ (0.065 g, 0.381 mmol), $TbCl_3$ (0.086 g, 0.324 mmol), dap (0.10 mL, 1.201 mmol) and H_2O (5 mL, 278 mmol) was stirred for 2 h, sealed in a 25 mL Teflon-lined steel autoclave, kept at 160 °C for 5 d and then cooled to room temperature. Purple prismatic crystals were obtained by filtering, washed with distilled water and then dried in air at ambient temperature. Yield: ca. 33% (based on $K_8Na_2[A\text{-}\alpha\text{-}GeW_9O_{34}]\cdot 25H_2O$). Anal. calcd. (found %) for $C_{12}H_{56}Cu_{1.50}GeN_8O_{46}TbW_{11}$ (**6**): C 4.24 (4.17), H 1.66 (1.79), N 3.30 (3.48), Cu 2.80 (2.91), Ge 2.14 (2.30), Tb 4.68 (4.56), W 59.52 (59.61). IR (KBr pellets, cm^{-1}): 3477(vs), 3308(w), 3255(w), 3143(w), 2970 (w), 2931(w), 1619(m), 1588(m), 1460(w), 1398(w), 1165(w), 1064(m), 1020(m), 943(s), 877(vs), 813(vs), 768(vs), 697(s) (Fig. S1A, S1B).

$[H_2dap][Cu(dap)_2(H_2O)][Cu(dap)_2]_{0.5}[Er(H_2O)_3(\alpha\text{-}GeW_{11}O_{39})]\cdot 3H_2O$ (7). A mixture of $K_8Na_2[A\text{-}\alpha\text{-}GeW_9O_{34}]\cdot 25H_2O$ (0.307 g, 0.099 mmol), $CuCl_2\cdot 2H_2O$ (0.098 g, 0.575 mmol),

Table 1 X-ray diffraction crystallographic data and structure refinements for **1**–**7**

	1	**2**	**3**	**4**	**5**	**6**	**7**
Empirical formula	$C_{12}H_{56}Cu_{1.5}GeLaN_8O_{46}W_{11}$	$C_{12}H_{56}Cu_{1.50}GePrN_8O_{46}W_{11}$	$C_{12}H_{56}Cu_{1.5}GeNdN_8O_{46}W_{11}$	$C_{12}H_{56}Cu_{1.50}GeSmN_8O_{46}W_{11}$	$C_{12}H_{56}Cu_{1.50}GeEuN_8O_{46}W_{11}$	$C_{12}H_{56}Cu_{1.50}GeTbN_8O_{46}W_{11}$	$C_{12}H_{56}Cu_{1.50}GeErN_8O_{46}W_{11}$
Formula weight	3377.81	3379.73	3383.14	3389.25	3390.86	3397.72	3406.16
Crystal system	triclinic	triclinic	triclinic	triclinic	triclinic	triclinic	triclinic
Space group	*P*–1	*P*–1	*P*–1	*P*–1	*P*–1	*P*–1	*P*–1
a, Å	11.5054(11)	11.430(2)	11.4615(14)	11.408(3)	11.327(6)	11.472(5)	11.2900(8)
b, Å	12.5391(12)	12.540(3)	12.6091(15)	12.563(4)	12.493(6)	12.626(6)	12.4765(9)
c, Å	21.400(2)	21.298(4)	21.456(3)	21.400(6)	21.298(10)	21.551(10)	21.3987(15)
α, deg	86.083(2)	85.591(4)	85.706(2)	85.602(5)	85.454(9)	85.036(7)	84.6320(10)
β, deg	76.139(2)	76.173(4)	76.120(2)	75.868(5)	75.769(12)	75.206(7)	74.8200(10)
γ, deg	74.298(2)	73.999(4)	74.166(2)	74.308(5)	74.292(11)	74.721(7)	75.3590(10)
V , Å^{-3}	2885.6(5)	2849.2(10)	2895.9(6)	2863.3(14)	2812(2)	2911(2)	2813.4(3)
Z	2	2	2	2	2	2	2
μ, mm^{-1}	23.702	24.110	23.776	24.166	24.679	23.980	25.043
F(000)	2997	3000	3003	3007	3009	3033	3019
T, K	296(2)	296(2)	296(2)	296(2)	296(2)	296(2)	296(2)
Limiting indices	$-13 \le h \le 13$ $-14 \le k \le 14$ $-24 \le l \le 25$	$-12 \le h \le 13$ $-14 \le k \le 14$ $-25 \le l \le 24$	$-13 \le h \le 13$ $-14 \le k \le 14$ $-18 \le l \le 25$	$-13 \le h \le 13$ $-14 \le k \le 14$ $-17 \le l \le 25$	$-10 \le h \le 13$ $-13 \le k \le 14$ $-24 \le l \le 25$	$-13 \le h \le 13$ $-15 \le k \le 14$ $-21 \le l \le 25$	$-13 \le h \le 12$ $-14 \le k \le 14$ $-22 \le l \le 25$
No. of reflections collected	14704	14412	14273	14149	14237	14707	14387
No.of independent reflections	10036	9919	9943	9897	9798	10105	9717
R_{int}	0.0534	0.0316	0.0590	0.0922	0.1504	0.0532	0.1150
Data/restrains/parameters	10036/170/657	9919/25/672	9943/86/672	9897/149/632	9798/208/587	10105/11/658	9717/89/658
GOFon F^2	0.990	1.016	1.034	1.005	0.997	1.032	1.000
Final *R* indices [$I>2\sigma(I)$]	[a]R_1 = 0.0622 [b]wR_2 = 0.1600	R_1 = 0.0477, wR_2 = 0.1143	R_1 = 0.0735 wR_2 = 0.1858	R_1 = 0.0964 wR_2 = 0.2208	R_1 = 0.1131 wR_2 = 0.1712	R_1 = 0.0614 wR_2 = 0.1594	R_1 = 0.0637 wR_2 = 0.1801
R indices (all data)	R_1 = 0.0815 wR_2 = 0.1726	R_1 = 0.0705 wR_2 = 0.1220	R_1 = 0.0896 wR_2 = 0.1956	R_1 = 0.1474 wR_2 = 0.2491	R_1 = 0.2430 wR_2 = 0.1969	R_1 = 0.0731 wR_2 = 0.1675	R_1 = 0.0715 wR_2 = 0.1866
Largest diff. peak and hole, e·Å^{-3}	3.588, –3.868	2.551, –3.169	4.429, –5.716	4.273, –4.501	3.422, –4.412	3.799, –4.266	4.486, –4.381

[a]$R_1 = \sum||F_o| - |F_c||/\sum|F_o|$. [b]$wR_2 = [\sum w(F_o^2 - F_c^2)^2/\sum w(F_o^2)^2]^{1/2}$; $w = 1/[\sigma^2(F_o^2) + (xP)^2 + yP]$, $P = (F_o^2 + 2F_c^2)/3$, where x = 0.0999, y = 0.0000 for **1**; x = 0.0601, y = 0.0000 for **2**; x = 0.1070, y = 0.0000 for **3**; x = 0.0368, y = 0.0000 for **4**; x = 0.0267, y = 0.0000 for **5**; x = 0.0958, y = 0.0000 for **6**; x = 0.1413, y = 0.0000 for **7**.

$ErCl_3$ (0.107 g, 0.391 mmol), dap (0.10 mL, 1.201 mmol) and H_2O (5 mL, 278 mmol) was stirred for 2 h, sealed in a 25 mL Teflon-lined steel autoclave, kept at 160 °C for 5 d and then cooled to room temperature. Purple prismatic crystals were obtained by filtering, washed with distilled water and then dried in air at ambient temperature. Yield: ca. 33% (based on $K_8Na_2[A\text{-}\alpha\text{-}GeW_9O_{34}]\cdot 25H_2O$). Anal. calcd. (found %) for $C_{12}H_{56}Cu_{1.50}GeN_8O_{46}ErW_{11}$ (**7**): C 4.23 (4.34), H 1.66 (1.81), N 3.29 (3.14), Cu 2.80 (2.91), Er 4.91 (4.80), Ge 2.13 (2.04), W 59.37 (59.03). IR (KBr pellets, cm^{-1}): 3486(vs), 3307(w), 3258(w), 3143(w), 2970(w), 2930(w), 1620(m), 1587(m), 1461(w), 1384(w), 1175(w), 1065(m),
1019 (m), 944(s), 879(vs), 812(vs), 767(vs), 695(s) (Fig. S1A, S1B).

Preparations of 3- and 4-CPE

3-modified CPE (**3**-CPE) was fabricated as follows: 30 mg of graphite powder and 10 mg of **3** were mixed and ground together by an agate mortar and pestle to achieve a uniform mixture, and then 0.05 mL of paraffin oil was added with stirring. The homogenized mixture was packed into a glass tube with a 3.0 mm inner diameter, and the tube surface was wiped with paper. Electrical contact was established with a Cu rod through the back of the electrode. In a similar manner, **4**-CPE was made with **4**.

X-ray crystallography

Intensity data for **1–7** were collected on a Bruker APEX–II CCD detector at 296(2) K with Mo Kα radiation (λ = 0.71073 Å).Direct methods were used to solve their structures and to locate the heavy atoms using the SHELXTL–97 program package.[14] The remaining non-hydrogen atoms were found from successive difference Fourier syntheses and full-matrix least-squares refinements on F^2. Lorentz polarization and empirical absorption corrections were applied. No hydrogen atoms associated with water molecules were located from the difference Fourier map. The positions of hydrogen atoms attached to carbon and nitrogen atoms were geometrically placed. All hydrogen atoms were refined isotropically as a riding model using the default SHELXTL parameters. All the non-hydrogen atoms were anisotropically refined except for some water molecules, oxygen, carbon and nitrogen atoms (details are seen in ESI). Crystallographic data and structure refinements for **1–7** are summarized in Table 1. Crystallographic data for the structures reported in this paper have been deposited in the Cambridge Crystallographic Data Centre with CCDC 967043, 967044, 967042, 967045, 967046, 967047and 967048 for **1**, **2**, **3**, **4**, **5**, **6** and **7**, respectively.These data can be obtained free of charge from the Cambridge Crystallographic Data Centre via www.ccdc.cam.ac.uk/data_request/cif.

Results and discussion

Syntheses

1–7 were obtained from the reaction of lacunary GT precursor [α-A-GeW_9O_{34}]$^{10-}$ with Cu^{II} and Ln^{III} cations in the participation of dap under hydrothermally conditions. Though the trivacant Keggin [α-A-GeW_9O_{34}]$^{10-}$ precursor has been intensively exploited since 2004,[11] investigations on the reactions of the [α- A-GeW_9O_{34}]$^{10-}$ precursor, TM and Ln cations are rare. Considering the advantages of hydrothermal conditions, the flexibility of various coordination modes and the Jahn-Teller effect of Cu^{II} ions, and the oxophilicity and high coordination numbers of Ln^{III} cations, the system including [α-A-GeW_9O_{34}]$^{10-}$, Cu^{II} and Ln^{III} was developed and some neoteric Cu–Ln containing GTs were made.[12] Three double {Cu_3LnO_4} cubane inserted GTs {[$Cu(en)_2(H_2O)$][$Cu_3Ln(en)_3(OH)_3(H_2O)_2$](α-$GeW_{11}O_{39}$)}$_2$·$nH_2O$ (Ln = Eu^{III}, n = 11; Ln = Tb^{III}, n = 11; Ln = Dy^{III}, n = 10) and three tetrameric architectures {$Cu(en)_2$[Ln(α-$GeW_{11}O_{39})_2$]$_2$}$^{24-}$ (Ln = La^{III}, Pr^{III}, Er^{III}) built by two 1:2-type [Ln(α-$GeW_{11}O_{39})_2$]$^{13-}$ moieties via a $[Cu(en)_2]^{2+}$ bridge were first obtained.[12a] When Gd^{III} or Y^{III} cations were introduced to the system, two tetrahedral PBTLHD nanoclusters $Na_3H_7[Cu(en)_2]_5[Cu(en)_2(H_2O)]_2[RE_4Ge_4W_{46}O_{164}(H_2O)_3]\cdot nH_2O$ (RE = Gd^{III}, n = 25; RE = Y^{III}, n = 23) were synthesized.[12b] As ongoing efforts to this branch, when dap replaced en, seven isomorphous Cu^{II}–Ln^{III} containing GTs **1**–**7** were sequentially separated, whose main skeletons are constructed from the 1-D Cu^{II}–Ln^{III} heterometallic GT double-chains by means of the bridging role of $[Cu(dap)_2]^{2+}$ cations. From the above results, several points can be mentioned here: (a) All Cu^{II}–Ln^{III} containing GTs prepared by us consist of [α-$GeW_{11}O_{39}$]$^{8-}$ fragments although we used the [α-A-GeW_9O_{34}]$^{10-}$ precursor, indicating that it is favorable for conversion from [α-A-GeW_9O_{34}]$^{10-}$ to [α-$GeW_{11}O_{39}$]$^{8-}$ during the course of formation. When K_6Na_2[α-$GeW_{11}O_{39}$]·$13H_2O$ replaced K_8Na_2[A-α-GeW_9O_{34}]·$25H_2O$ under similar conditions, the same target products can be not afforded, which can further support this proposal. (b) Organic ligands have an important influence on the structural constructions of the outcomes. When dap replaced en, we obtained 1-D double-chain Cu^{II}–Ln^{III} heterometallic GTs reported in this paper. (c) The nature of Ln^{III} ions greatly affects structural constructions in the [α-A-GeW_9O_{34}]$^{10-}$, Cu^{II}, Ln^{III} and en system whereas the nature of Ln^{III} ions has no obvious effect on structural constructions in the [α-A-GeW_9O_{34}]$^{10-}$, Cu^{II}, Ln^{III} and dap system. For example, in the presence of en, double {Cu_3LnO_4} cubane inserted GTs were made for Eu^{III}, Tb^{III} and Dy^{III} cations, tetrameric {$Cu(en)_2$[Ln(α-$GeW_{11}O_{39})_2$]$_2$}$^{24-}$ were formed for La^{III}, Pr^{III} and Er^{III} cations while copper-bridged tetrahedral PBTLHD nanoclusters are only formed by virtue of Gd^{III} or Y^{III} cations. In the participation of dap, only 1-D double-chain Cu^{II}–Ln^{III} heterometallic GTs were obtained. (d) The nature of TM cations can also influence the structural diversity of the products. Ni^{II} or Co^{II} were used in the presence of Ln^{III} ions under similar conditions, unfortunately, only organic–inorganic hybrid TM substituted GTs $[enH_2]_2$ $[Ni(en)_2]_2${$[Ni_6(en)_2(H_2O)_2]$[B-α-$GeW_9O_{34}]_2$}·$14H_2O$,[15a] and {[Co $(dap)_2(H_2O)]_2$[$Co(dap)_2]_2$[$Co_4(Hdap)_2$(B-α-$HGeW_9O_{34})_2$]}·$7H_2O$ [15b] were obtained. When other TM ions such as Ti^{4+}, Cr^{3+}, Fe^{2+} and Cd^{2+} ions were used, however, amorphous powders were obtained. In the future, we will introduce other functional organic ligands such as aliphatic polycarboxylic acid and aromatic polycarboxylic acid ligands to the system to prepare much more TM–Ln containing GTs with excellent properties and novel architectures.

Structural descriptions

Bond valence sum (BVS) calculations [17a–c] of **1–7** indicate that the oxidation states of all W, Cu and Ln atoms are +6, +2 and +3, respectively (Table S1) and **1**, **3**, **5** and **7** are further confirmed by XPS spectra (Fig. 2, S2). The $W4f_{7/2}$ and $W4f_{5/2}$ binding energies of 34.0 and 35.7 eV for **1**, 33.5 and 35.6 eV for **3**, 34.0 and 35.9 eV for **5**, 33.8 and 35.9 for **7** are coincident with the previous results,[18a–c] which indicate that all the W centers are +6 in **1**, **3**, **5**, **7**. The spin–orbit components ($2p_{3/2}$ and $2p_{1/2}$) of the Cu2p peak are well deconvoluted by two curves at 932.9 and 952.6 eV for **1**, 932.8 and 952.0 eV for **3**, 932.8 and 953.2 eV for **5**, 933.3 and 953.0 eV for **7.** These values are in line with the reported values,[18d] confirming the presence of the Cu^{II} cations in **1**, **3**, **5** and **7**. Two peaks at 833.4 and 853.6 eV correspond to the $La3d_{5/2}$ and $La3d_{3/2}$ of the La^{III} cation in **1**.[18e] The peaks at 979.9 and 1003.7 eV are ascribed to the $Nd3d_{5/2}$ and $Nd3d_{3/2}$ of the Nd^{III} cation in **3**.[18f] In **5**, the XPS profile exhibits two peaks at 1132.3 and 1162.0 eV, which are assigned to the $3d_{5/2}$ and $3d_{3/2}$ levels of the Eu^{III} cation.[18g] The $Er^{III}4d_{3/2}$ peak is found at 170.4 eV.[18f] These results are consistent with BVS calculations from the X-ray structural analysis data.

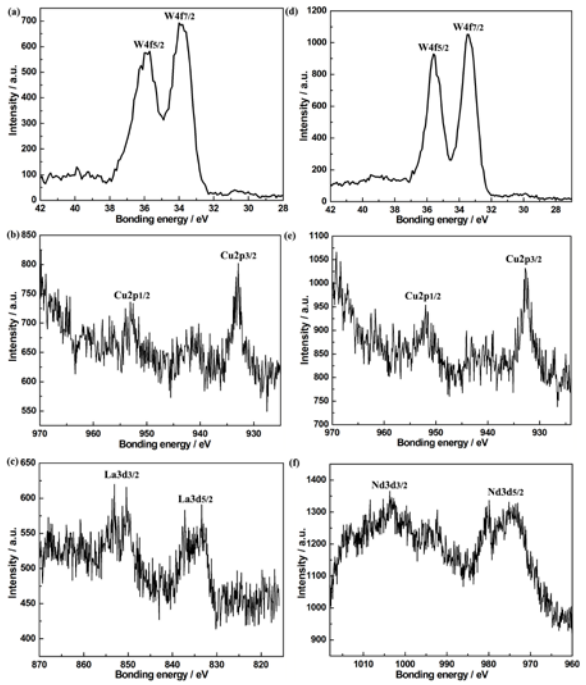

Fig. 2 a) The XPS spectrum for $W4f_{7/2}$ and $W4f_{5/2}$ in **1**; b) The XPS spectrum for $Cu2p_{3/2}$ and $Cu2p_{1/2}$ in **1**; c) The XPS spectrum for $La3d_{5/2}$ and $La3d_{3/2}$ in **1**; d) The XPS spectrum for $W4f_{7/2}$ and $W4f_{5/2}$ in **3**; e) The XPS spectrum for $Cu2p_{3/2}$ and $Cu2p_{1/2}$ in **3**; f) The XPS spectrum for $Nd3d_{5/2}$ and $Nd3d_{3/2}$ in **3**.

The phase purity of **1–7** is supported by the agreement of the PXRD patterns of the bulks with the calculated patterns from the single-crystal structural analyses (Fig. S3,S4). The intensity differences between experimental and simulated PXRD patterns are due to the variation in preferred orientation of the powder sample during collection of the experimental PXRD. Single-crystal X-ray structural analyses display that **1–7** are isomorphic and all crystallize in the triclinic space group *P*–1. **1–7** all display a 1-D double-chain architecture formed by two 1-D antiparallel Cu^{II}–Ln^{III} heterometallic GT polymeric chains $\{[Cu(dap)_2(H_2O)][Ln(H_2O)_3(\alpha\text{-}GeW_{11}O_{39})]\}_n^{3n-}$ by means of the bridging functionality of the $[Cu(dap)_2]^{2+}$ cations. Herein, only the structure of **1** is described in details. Additionally, because of the existence of the Jahn–Teller effect of Cu^{II} ions in the ligand field resulting in the elongation of the Cu–O distances, the Cu–O weak interactions will be considered in the following description. The asymmetrical structural unit $[H_2dap][Cu(dap)_2]_{0.5}[Cu(dap)_2(H_2O)][Ln(H_2O)_3(\alpha\text{-}GeW_{11}O_{39})]\cdot 3H_2O$ of **1** (Fig. 3a) consists of a mono-La^{III} substituted Keggin-type $[Ln(H_2O)_3(\alpha\text{-}GeW_{11}O_{39})]^{5-}$subunit, half $[Cu(dap)_2]^{2+}$ bridging cation, one pendent $[Cu(dap)_2(H_2O)]^{2+}$ cation, a diprotonated $[H_2dap]^{2+}$ and three lattice water molecules. In the asymmetrical structural unit, the pendent $[Cu1(dap)_2(H_2O)]^{2+}$ cation links to the $[Ln(H_2O)_3(\alpha\text{-}GeW_{11}O_{39})]^{5-}$ subunit via a terminal oxygen atom and is embedded in a severely distorted octahedral geometry, in which four nitrogen atoms from two dap ligands occupy the basal plane [Cu–N: 1.993(19)–2.022(18) Å] and a terminal oxygen atom [Cu–O: 3.277(11) Å] and a water ligand [Cu–O: 2.321(16) Å] stand on two axial positions. The bridging $[Cu2(dap)_2]^{2+}$ cation is located on the special site with the atomic coordinate (0.5, 0.5, 0) leading to an occupancy of 50% and inhabits in an elongated octahedron defined by four nitrogen atoms from two dap ligands with Cu–N distances of 1.97(3)–1.99(3) Å building the equatorial plane and two oxygen

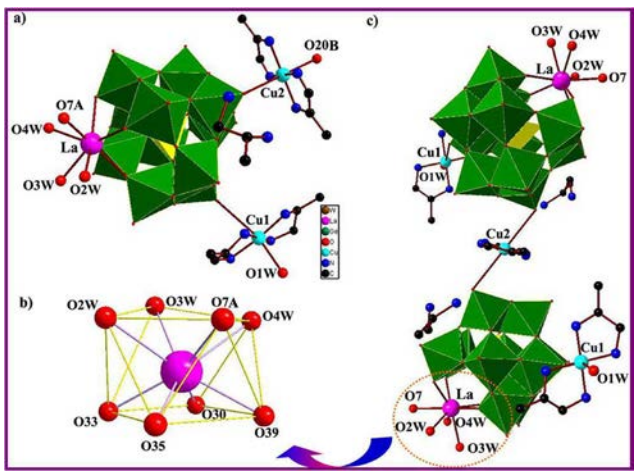

Fig. 3 a) The asymmetrical structural unit of **1** with the selected numbering scheme; b) The eight-coordinate distorted square antiprism of the La^{III} cation; c) The dimeric structural unit made up of two $[Cu(dap)_2(H_2O)][La(H_2O)_3(\alpha\text{-}GeW_{11}O_{39})]^{3-}$ moities though a $[Cu2(dap)_2]^{2+}$ linker. The atoms with "A, B" labels are symmetrically generated (A: 1 + *x*, *y*, *z*; B: 1 – *x*, 1 – *y*, –*z*). Hydrogen atoms, protons and lattice water molecules are omitted for clarity.

atoms from two adjacent $[Ln(H_2O)_3(\alpha\text{-}GeW_{11}O_{39})]^{5-}$ subunits with long Cu–O distances of 3.310(42) Å occupying two polar sites. The $[Cu1(dap)_2(H_2O)]^{2+}$ and $[Cu2(dap)_2]^{2+}$ cations display elongated octahedral geometries, proving the occurrence of Jahn–Teller distortion of the copper cations in the ligand field,[19] which can be inferred that both Cu1 and Cu2 cations adopt the electron configuration of $(t_{2g})^6(d_{x2\text{-}y2})^1(d_{z2})^2$. The La^{III} cation is captured by the monovacant $[\alpha\text{-}GeW_{11}O_{39}]^{8-}$ fragment and resides in an eight-coordinate distorted square antiprismatic geometry (Fig. 3b). The La^{III} cation is coordinated by eight oxygen atoms, four of which come from one $[\alpha\text{-}GeW_{11}O_{39}]^{8-}$ fragment [La–O: 2.428(14)–2.488 (13) Å], one from the other neighboring $[\alpha\text{-}GeW_{11}O_{39}]^{8-}$fragment [La–O: 2.526(15) Å]. In the coordinate polyhedron around the La^{III} cation, the O7, O2W, O3W and O4W group and the O30, O33, O35 and O39 group constitute two bottom planes of the square antiprism and the average deviations from their ideal planes are 0.1012 and 0.0072 Å, respectively. The distances between the La cation and two bottom planes are 1.4911 and 1.1312 Å, respectively. Especially, the La–O7 distance of 2.526(15) Å is much longer than those of the other La–O bonds (La–O30, La–O33, La–O35, La–O39) distances because the W–O–La–O7–W linkage participates in the construction of the 1-D chain (Fig. 4a). More interesting is that two asymmetrical structural units of **1** are joined together by means of the $[Cu2(dap)_2]^{2+}$ cation constructing the dimeric structural unit $\{[Cu(dap)_2(H_2O)][La(H_2O)_3(\alpha\text{-}GeW_{11}O_{39})]\}_2^{6-}$ (Fig. 3c). The most remarkable structural characteristic of

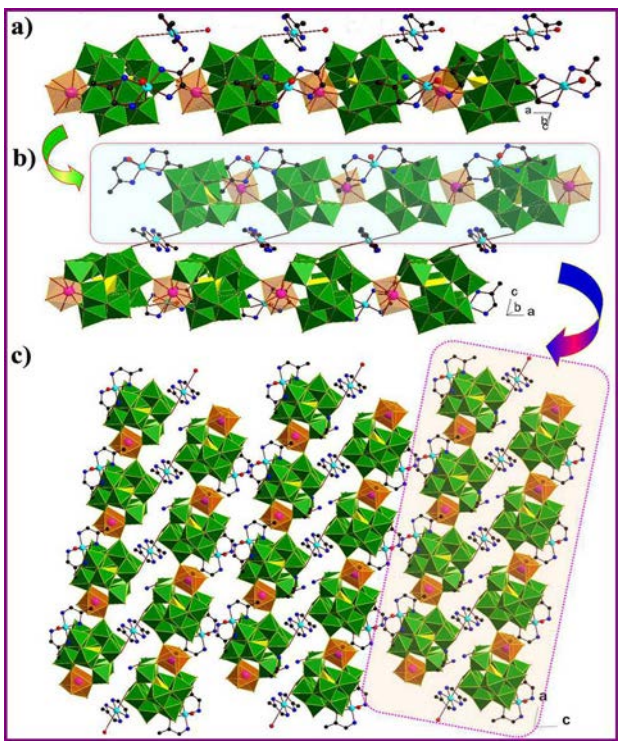

Fig. 4 a) The 1-D chain constructed by the W–O–La–O7–W linkers in **1**;

b) The 1-D organic–inorganic hybrid double-chain architecture of **1**; c) Arrangement of 1-D double-chains in the crystallographic ac plane in **1** showing the mode of –AAA–.

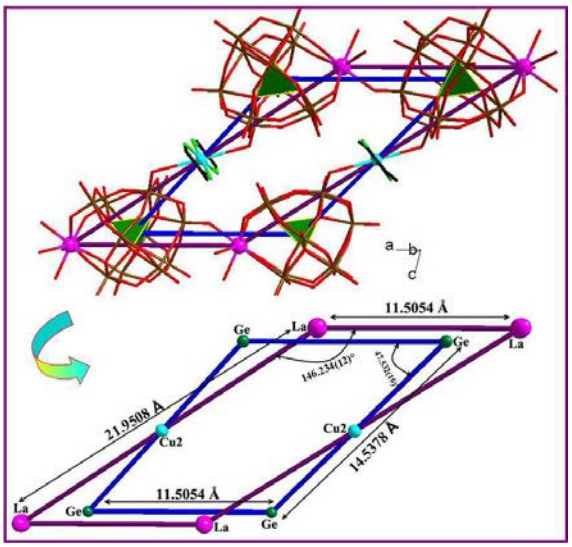

Fig. 5 Two parallelograms in the structure.

1 is that each dimeric structural unit $\{[Cu(dap)_2(H_2O)][La(H_2O)_3(\alpha\text{-}GeW_{11}O_{39})]\}_2^{6-}$ connects two adjacent identical units through four W–O–La–O–W bridges and construct the beauteous 1-D antiparallel double-chain motif (Fig. 4b). Alternatively, the 1-D antiparallel double-chain structure can be also viewed as a fusion of two 1-D linear chains $\{[Cu(dap)_2(H_2O)]La(H_2O)_3(\alpha\text{-}GeW_{11}O_{39})]\}_n^{3n-}$ formed by asymmetrical structural units $\{[Cu(dap)_2(H_2O)][La(H_2O)_3(\alpha\text{-}GeW_{11}O_{39})]\}^{3-}$ via $[Cu2(dap)_2]^{2+}$ linkers (Fig. 4a,4b). Actually, other 1-D polymeric chains created by mono-Ln substituted Keggin moieties have been previously observed. For example, in 2000, Pope and co-workers communicated two 1-D inorganic zigzag chain-like Ln-containing monovacant Keggin silicotungstates $[Ln(\alpha\text{-}SiW_{11}O_{39})(H_2O)_3]^{5-}$ (Ln = Ce^{III}; La^{III});[20a] In 2003, Mialane et.al. discovered a 1-D inorganic linear $[Yb(\alpha\text{-}SiW_{11}O_{39})(H_2O)_2]^{5-}$ chain and a 1-D zigzag $[Nd_2(\alpha\text{-}SiW_{11}O_{39})(H_2O)_{11}]^{2-}$ chain;[20b] Later, Niu et al. reported a 1-D inorganic /organic–inorganic zigzag chain $K_3\{[Pr(H_2O)_4(\alpha\text{-}SiW_{11}O_{39})](NaPr_2(H_2O)_{12})[Pr(H_2O)_4(\alpha\text{-}SiW_{11}O_{39})]\}\cdot 13H_2O$,[20c] $(CH_3)_4N]_{2.5}H_{2.5}[Y(GeW_{11}O_{39})(H_2O)_2]\cdot 4H_2O$,[20d] and $\{Dy(H_2O)_7[Dy(H_2O)_2(DMSO)(\alpha\text{-}GeW_{11}O_{39})]\}^{2-}$.[20e] To the best of our knowledge, **1-7** are the first organic–inorganic hybrid 1-D double-chain Cu^{II}–Ln^{III} heterometallic GTs albeit a GT-based Sm^{III}-containing 1-D double-chain GT $[Sm_2(\alpha\text{-}GeW_{11}O_{39})(DMSO)_3(H_2O)_6]^{2-}$,[20d] and inorganic 1-D Cr^{III}–La^{III} heterometallic double-chain silicotungstate $[(\gamma\text{-}SiW_{10}O_{36})_2(Cr(OH)(H_2O))_3(La(H_2O)_7)_2]^{4-}$[20f] have been addressed. It should be mentioned that there are two types of parallelograms in the double-chain structure of **1** (Fig. 5), the violet parallelogram with the side lengths of 21.9508 × 11.5054 Å and the inner angle of 146.234(12)° is made up of four La^{III} cations from two dimeric structural units $\{[Cu(dap)_2(H_2O)][La(H_2O)_3(\alpha\text{-}GeW_{11}O_{39})]\}_2^{6-}$ and the blue parallelogram with the side lengths of 14.5378 × 11.5054 Å and the inner angle of 47.532(16)° is constituted by four Ge^{IV} atoms from two dimeric structural units $\{[Cu(dap)_2\ (H_2O)][La(H_2O)_3(\alpha\text{-}GeW_{11}O_{39})]\}_2^{6-}$. The intersection line of two parallelograms passes through two Cu2 cations and their dihedral angle is 2.38°, which indicates that La^{III} cations are not fully incorporated to the monovacant site of $[\alpha\text{-}GeW_{11}O_{39}]^{8-}$ fragments. This case not only is related to the atom radius of the La^{III} cation being larger than that the W center but also is in relation to the bridging role of La^{III} cations in the construction of the 1-D linear chain $\{[Cu(dap)_2(H_2O)][La(H_2O)_3(\alpha\text{-}GeW_{11}O_{39})]\}_n^{3n-}$. In addition, the 1-D double chains in **1** are aligned in the arrangement mode of –AAA– (Fig. 4c, S5).

It should be pointed out that the design and assembly of metal-involved supramolecular architectures are currently of great interest in supramelocular chemistry and crystal engineering because they can provide novel topology and functional materials.[21] Moreover, Keggin-based supramolecular architectures are regarded as one of the most promising materials potentially applied in the field of chemistry, biology and material sciences.[22] From the viewpoint of supramelocular chemistry, supramolecular structures are also present in **1–7** considering hydrogen bonding interactions between nitrogen atoms of dap ligands and surface oxygen atoms of POM units and water molecules. Specifically speaking, dap ligands work as the proton donors, surface oxygen atoms of mono-RE substituted Keggin GTs and water molecules function as the proton acceptors, and then donors and acceptors are hydrogen-bonded together generating the infinitely 3-D supramolecular architectures (Fig. 6). The N–H···O distances are in the range of 2.67(3)–3.48(4) Å for **1**, 2.859(19)–3.51(2) Å for **2**, 2.87(3)–3.54(3) Å for **3**, 2.83(4)–3.41(4) Å for **4**, 2.64(6)–3.43(5) Å for **5**, 2.59(3)–3.47(3) Å for **6**, and 2.90(2)–3.35(4) Å for **7**, respectively.

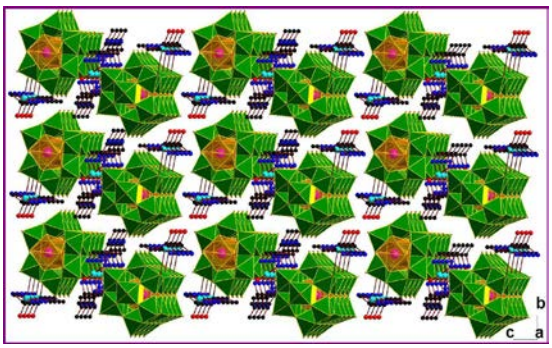

Fig. 6 The 3-D extended supramolecular architecture of **1**.

IR spectra

IR spectra for **1–7** were recorded as KBr pellets in the range of 4000–400 cm^{-1} (Fig. S1A, S1B). Their IR spectra display the characteristic vibration patterns resulting from the Keggin POT framework in the region of 1100–600 cm^{-1}. Four characteristic vibration bands attributable to $\nu_{as}(Ge–O_a)$, terminal $\nu_{as}(W–O_t)$, corner-sharing

ν_{as}(W–O_b), and edge-sharing ν_{as}(W–O_c) asymmetric vibrations derived from the Keggin GT framework, appear at 879–873, 944–940, 814–810, 769–766 and 697–692 cm^{-1}, respectively. Specifically, four groups of characteristic vibration bands corresponding to ν(Ge–O_a), ν(W–O_t), ν(W–O_b), and ν(W–O_c) are observed at 873; 940; 811; 767; and 692 cm^{-1} for **1**, 876; 939; 813; 767; and 693 cm^{-1} for **2**, 876; 941; 876; 813; 767; and 695 cm^{-1} for **3**, 876; 941; 814; 769; and 695 cm^{-1} for **4**, 875; 942; 810; 766; and 693 cm^{-1} for **5**, 877; 943; 813; 768; and 697 cm^{-1} for **6**, 879; 944; 812; 767; and 695 cm^{-1} for **7**, respectively. In general, these characteristic bands can be easily assigned in comparison with the corresponding bands of monovacant Keggin POT clusters.[15,16a] Compared with the $K_6Na_2[\alpha\text{-}GeW_{11}O_{39}]\cdot 13H_2O$ precursor,[16b] the ν(W–O_t) vibration bands for **1–7** are almost not shift, suggesting the weak influence of $[Cu(dap)]^{2+}$ and $[Cu(dap)_2(H_2O)]^{2+}$ cations on the terminal oxygen atoms on the $[\alpha\text{-}GeW_{11}O_{39}]^{8-}$ fragments. This phenomenon can be also confirmed by the long Cu–O_t distances (> 2.5 Å) from the X-ray single crystal analyses. Furthermore, the possible major reason that the ν(W–O_b) split into two bands may be related to the fact that the incorporation of the Ln cations to the defect sites of $[\alpha\text{-}GeW_{11}O_{39}]^{8-}$ fragments lead to the deformation and distortion of the $[\alpha\text{-}GeW_{11}O_{39}]^{8-}$ skeletons. In addition, the stretching bands of –OH, $–NH_2$ and $–CH_2$ groups are observed at 3486–3461, 3308–3140 and 2971–2928 cm^{-1}, respectively. The bending vibration bands of $–NH_2$ and $–CH_2$ groups appear at 1621–1522 and 1493–1461 cm^{-1}, respectively. The occurrence of these characteristic signals confirms the presence of organic amine groups and water molecules in **1–7**, which is in good agreement with the single-crystal structural analyses.

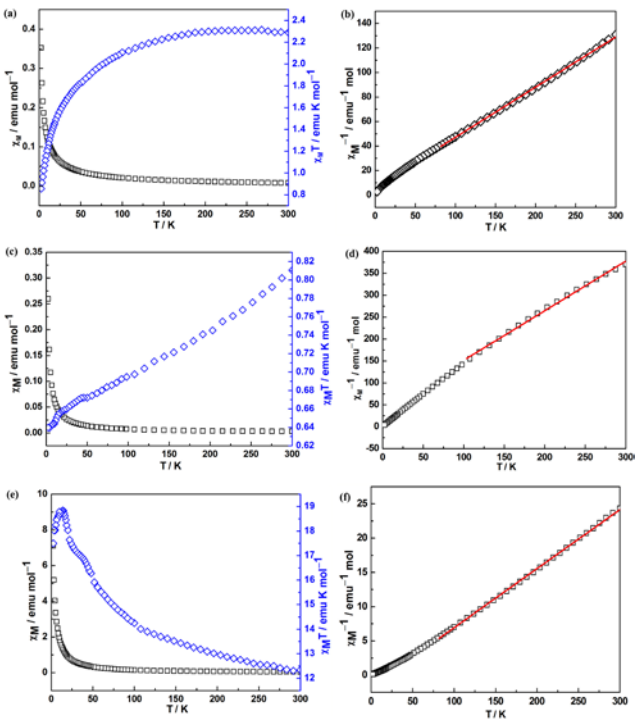

Fig. 7 a) Temperature dependence of magnetic susceptibility for **2** between 2 and 300 K; b) Temperature evolution of the inverse magnetic susceptibility for **2** between 80 and 300 K; c) Temperature dependence of magnetic susceptibility for **4** between 2 and 300 K; d) Temperature evolution of the inverse magnetic susceptibility for **4** between 100 and 300 K; e) Temperature dependence of magnetic susceptibility for **7** between 2 and 300 K; f) Temperature evolution of the inverse magnetic susceptibility for **7** between 80 and 300 K. The red solid lines were generated from the best fit by the Curie–Weiss expression.

Magnetic properties

Recently, the research and discovery of TM–Ln containing complexes with magnetic interactions in the solid-state chemistry and material science have been attracted increasing attention.[23] Though lots of TM–Ln containing complexes have been reported, except for the isotropic Gd^{III} cation having an f^7 electron configuration and an orbitally non-degenerate ground state, not much is known about the nature and magnitude of the exchange interaction of Ln cations between themselves and with other magnetic groups and the evolution of the magnetic properties along the Ln series,[24a] because the magnetic properties of Ln cations are strongly influenced by spin–orbit couplings and in particular the magnetocrystalline anisotropy is generally large.[24b,c] Generally, the orbital component of the magnetic moment is much more important for Ln cations compared to TM cations, since ligand-field effects are smaller and spin–orbit couplings larger for f electrons of Ln cations.[25a] Under the influence of the interelectronic repulsion and spin–orbit couplings, the ^{2S+1}L group term of the $4f^n$ configuration of Ln cations are split into $^{2S+1}L_J$ spectroscopic levels. Each of these states is further split into Stark sublevels by the ligand-field perturbation.[24a] Although the theory of the paramagnetic properties of Ln cations has long been investigated, the presence of the large unquenched orbital angular momentum has not allowed the development of simple models for a rational analysis of the structural magnetic correlations.[24c] Since there are Cu^{III} and Ln^{III} centers in **1–7**, the magnetic susceptibilities of **2**, **4** and **7** have been measured on their polycrystalline samples in an applied magnetic field of 2000 Oe in the temperature range of 2–300 K (Fig. 7) on a Quantum Design MPMS XL–7 magnetometer.

In the case of **2**, the magnetic data for **2** are plotted in the form of χ_M and $\chi_M T$ versus T (Fig. 7a). The temperature dependence of χ_M exhibits a slightly increases from 0.01 emu mol^{-1} at 300 K to 0.05 emu mol^{-1} at 36 K. This tendency becomes more pronounced below 36 K, exponentially reaching 0.42 emu mol^{-1} at 2 K. Correspondingly, the $\chi_M T$ product at 300 K of 2.29 emu K mol^{-1} is consistent with the theoretical value (2.16 emu K mol^{-1}) expected for 1.5 non-interacting Cu^{II} cations (S = 1/2) considering g = 2 and 1 isolated Pr^{III} cations ($^3H_4$, J = 4, g = 4/5).[25b] The $\chi_M T$ value declines gradually between 300 and 34 K, where the $\chi_M T$ value is 1.69 emu K mol^{-1}. Blow 34 K, it falls sharply to 0.82 emu K mol^{-1} at 2 K. This decline phenomenon is related to the depopulation of the Stark levels of Pr^{III} cations upon cooling. It is well known that ligand-field effects can split the 9-fold degenerate $^3H_4$ ground state of the Pr^{III} cation into Stark levels and the value of $\chi_M T$ mainly depends on the populations of those Stark levels.[25c] As for **2**, at 300 K, all the Stark levels from the 9-

fold degenerate $^3H_4$ ground states are populated, such that $\chi_M T$ is equal to the value expected for one free Pr^{III} ion and one and a half isolated Cu^{II} cations, however, as temperature drops, the progressive depopulation of higher Stark levels occurs, leading to the decrease of the $\chi_M T$ value. The curve of χ_M^{-1} versus T between 80 and 300 K (Fig. 7b) follows the Curie–Weiss expression [$\chi_M = C/(T-\theta)$] with C = 2.44 emu K mol^{-1} and θ = –15.05 K for **2**. The larger θ value also indicates the importance of ligand-field effects in **2**.[25d] In the meantime, the progressive depopulation of higher Stark levels can also result in the deviation of the curve of χ_M^{-1} versus T to the Curie–Weiss law.

For **4**, the magnetic data are plotted in Fig. 7c in the form of χ_M and $\chi_M T$ versus T. The temperature dependence of χ_M exhibits a slight increase from 0.003 emu mol^{-1} at 300 K to 0.019 at 36 K and then exponentially to the maximal value of 0.321 emu mol^{-1} at 2 K. The $\chi_M T$ product at 300 K is 0.81 emu K mol^{-1}, being higher than the expected value of 0.65 emu K mol^{-1} for 1.5 isolated Cu^{II} cations with S = 1/2 and g = 2 and 1 free Sm^{III} cation ($^6H_{5/2}$, J = 5/2, g = 2/7).[25e] This suggests the existence of the thermal population of the higher energy state of the free Sm^{III} ion at room temperature. In general, the ^6H ground term for the free Sm^{III} ion in the crystal field is split into six states by spin–orbit coupling and the spin–orbit coupling parameter is 1200 cm^{-1}, which often lead to the thermal population of the high energy states.[25f,g] The $\chi_M T$ value decline from 300 to 2 K, finally reaches the minimum value of 0.64 emu K mol^{-1}, which illustrates the occurrence of the depopulation of the Kramers doublets of higher energy. Similar phenomenon have been observed in the Sm^{III}-containing complexes such as $[Sm_2(4\text{-cba})_6(phen)_2(H_2O)_2]$ and $[\{(\alpha\text{-}PW_{11}O_{39})Ln(H_2O)(\eta^2,\mu\text{-}1,1)\text{-}CH_3COO\}_2]^{10-}$.[25c,g] Actually, The curve of χ_M^{-1} versus T in 100–300 K for **4** can be described using the Curie–Weiss law with the C = 0.88 emu K mol^{-1} and θ = 33.89 K (Fig. 7d), but the depopulation of the Kramers doublets of higher energy upon cooling results in the deviation of the relation of χ_M^{-1} versus T between 100 and 2 K.

With respect to **7**, the χ_M value slowly increase from 0.04 emu mol^{-1} at 300 K to 0.42 emu mol^{-1} at 40 K and then exponentially reaches the maximum of 8.50 emu mol^{-1} at 2 K (Fig. 7e). The value of $\chi_M T$ at 300 K of 12.33 emu K mol^{-1} is in line with the sum (12.04 emu K mol^{-1}) of the contribution attributable to one and a half free Cu^{II} cations (S = 1/2) with g = 2.00 and one free Er^{III} cation in the $^4I_{15/2}$ group state (J = 15/2, g = 6/5).[25h–k] The $\chi_M T$ value increase to a maximum of 18.85 emu K mol^{-1} at 14 K upon cooling (Fig. 7e). This behavior may indicate that the S_{Er} = 11/2 local spins somewhat tend to align along the same direction. The $\chi_M T$ decreases on the decreasing temperature from 14 to 2 K. This behavior suggests the intermolecular interactions. The relationship of χ_M^{-1} versus T in 80–300 K can be described by the Curie–Weiss law with C = 11.60 emu K mol^{-1} and θ = –19.63 K (Fig. 7f). However, as the temperature decreases from 80 to 2 K, the relation of χ_M^{-1} versus T does not follow the Curie–Weiss law.

Electrochemical and electrocatalytic properties

POMs, as a large and rapidly growing class, can undergo reversible multi-electron redox process, and can be utilized as the chemically bulk-modified CPEs with many advantages of inexpensive, easy to handle, easy to prepare, so they have attracted much attention in electrochemical applications and the manufacture of chemically modified electrodes.[26] By means of cyclic voltammetry (CV), the solid-state electrochemical and electrocatalytic properties of **3** and **4** have been carried out in 0.5 mol·L^{-1} Na_2SO_4 + H_2SO_4 aqueous solution (a medium suitable for testing electro-catalytic processes) by entrapping them in a carbon paste electrode (CPE). The reproducibility of cyclic voltammograms indicates that **3**-

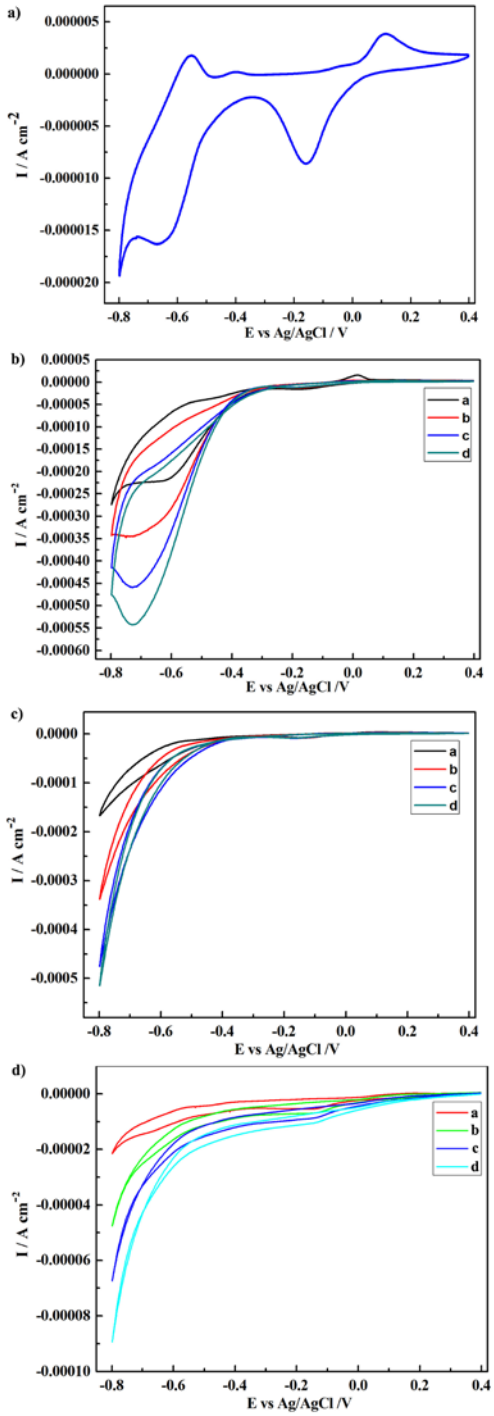

Fig. 8 a) Cyclic voltammogram of **3**-CPE in pH = 1.34 0.5 mol·L^{-1} Na_2SO_4 + H_2SO_4 aqueous solution; b) The evolution of cyclic voltammograms of **3**-CPE in pH = 1.34 0.5 mol·L^{-1} Na_2SO_4 + H_2SO_4 aqueous solution containing various H_2O_2 concentrations (a 5.88 × 10^{-3}, b 9.80 × 10^{-3}, c 1.37 × 10^{-2}, d 1.76 × 10^{-2} mol·L^{-1}); c) The evolution of cyclic voltammograms of **3**-CPE in pH = 1.34 0.5 mol·L^{-1} Na_2SO_4 + H_2SO_4 aqueous solution containing various $NaBrO_3$ concentrations (a 1 × 10^{-3}, b 3 × 10^{-3}, c 5 × 10^{-2}, d 7 × 10^{-3}), d) The evolution of cyclic voltammograms of **3**-CPE in pH = 1.34 0.5 mol·L^{-1} Na_2SO_4 + H_2SO_4 aqueous solution containing various $NaNO_2$ concentrations (a 3 × 10^{-3}, b 5 × 10^{-3}, c 7 × 10^{-3}, d 9 × 10^{-3} mol·L^{-1}). Scan rate: 50 mV s^{-1}.

CPE and **4**-CPE are stable in this medium. Since **3** and **4** are isostructural, their electrochemical and electro-catalytic properties are very similar (Fig. 8, S6). Since the pH value of the supporting electrolyte has a marked effect on the electrochemical behavior, we find that the best pH values of **3** and **4** are 1.34 and 1.35, respectively (Fig. S7, S8. Fig. 8a shows the typical CV behavior of **3** in a pH 1.34 sulfate medium (0.5 mol·L^{-1} Na_2SO_4 + H_2SO_4) at a scan rate of 50 mV s^{-1} at room temperature. The same to **4**, its typical CV behavior is illustrated in Fig. S6a. It can be clearly seen that in the potential range of –0.8 to 0.4 V, the CV patterns are restricted to two pairs of redox waves and their mean peak potentials $E_{1/2} = (E_{pa} + E_{pc}) / 2$ are –0.613 V and –0.023 V (vs the Ag/AgCl electrode) for **3**, and –0.548 V and 0.007 V(vs the Ag/AgCl electrode) for **4**, respectively. As expected, the W^{VI}-based wave is located at a more negative potential than that attributable to the Cu^{II} center. The former features the redox process of the W^{VI} centers and the latter is attributed to the redox process of the Cu^{II} center in the polyoxoanion framework.[13,26c]

Previous studies have shown that POMs are capable of delivering the electrons to other species, thus serving as the powerful electron reservoirs for multi-electron reductions and electrocatalytic processes.[27a] For example, Toth and Anson applied the iron^{III}-substituted Keggin type POMs as catalysts to the reductions of hydrogen peroxide and nitrite.[2b] Dong et al. observed that $[SiW_{12}O_{40}]^{4-}$ could be acted as an electrocatalyst for the reduction of nitrite.[27a] Here, **3**-CPE and **4**-CPE are employed to probe the electro-catalytic reductions of hydrogen peroxide, bromate and nitrite in 0.5 mol·L^{-1} Na_2SO_4 + H_2SO_4 aqueous solution (pH = 1.34 for **3** and pH = 1.35 for **4**). The H_2O_2 electro-activity improvement is of special interest for applications such as chemical industry, biosensors and fuel cells.[28a] Thus, the electro-catalytic investigations on the reduction of hydrogen peroxide catalyzed by other POMs have been performed. For a instance, in 2004, Wang's group firstly reported the high electrocatalytic reduction activity of hydrogen peroxide catalyzed by the Keggin-type phosphomolybdate (PMo_{12})-doped polypyrrole (PPy) CPE.[28b] In order to evaluate the electrocatalytic activity, **3**-CPE and **4**-CPE are employed to probe the electrocatalytic reduction of hydrogen peroxide (Fig. 8b, S6b). As shown in Fig. 8b and S6b, with the addition of hydrogen peroxide, the W^{VI}-based reduction peak currents increase, while the corresponding oxidation peak currents decrease. However, the Cu^{II} reduction wave is almost unaffected by addition of hydrogen peroxide. The results show that the reduction of nitrite is mainly mediated by the reduced species of tungsten-oxo clusters in **3** and **4**. To further illustrate their electrocatalytic potential, the reduction procedures of bromate catalyzed by them have been also carried out. The monitoring or removal of bromate species is interesting as it is present in drinking water samples as a byproduct of ozone disinfection and is often used as food additive.[12b] Moreover, the negative impacts of bromate on human body have been confirmed.[28c] As a result, developing new the rapid and inexpensive analytic methods to detect the presence of bromate is indispensable. So the electrocatalytic abilities of **3**-CPE and **4**-CPE toward the reduction of BrO_3^- have been studied in 0.5 mol·L^{-1} Na_2SO_4 + H_2SO_4 aqueous solution containing various $NaBrO_3$ concentrations at room temperature. Fig. 8c and S6c show the cyclic voltammograms for the electrocatalytic reduction of bromate by **3**-CPE and **4**-CPE. The catalytic effects of BrO_3^- are similar to the H_2O_2 for **3** and **4**, with addition of $NaBrO_3$, the reduction peak currents of the Cu^{II}-based wave is less affected wheras the W^{VI}-based reduction peak currents increase gradually and the corresponding oxidation peak currents gradually decrease, suggesting that the bromate is reduced by the species of tungsten components.[28d] Actually, such phenomenon has been previously encountered.[12b,28e–f] In addition, the electrocatalytic reduction of nitrite on **3**-CPE and **4**-CPE are also measured. The catalytic reduction evolution of nitrite on **3**-CPE and **4**-CPE can be seen clearly in Fig. 8d and S6d. Unlike the electrocatalytic reductions of hydrogen peroxide and bromate, the electrocatalytic reductions not only occurr on the W^{VI}-based wave obviously, but also appear on the Cu^{II}-based wave. With addition of $NaNO_2$, the reduction peak currents of the the W^{VI}-based wave and Cu^{II}-based wave increase steadily and their corresponding oxidation peak currents decrease The results show that the electrocatalytic reduction of nitrite is simutaneously mediated by the W^{VI}-based wave and Cu^{II}-based wave in **3** and **4**. As discussed above, **3** and **4** display apparent electro-catalytic activities for the nitrite, bromate and hydrogen peroxide reduction.

Conclusions

In conclusion, we have synthesized a family of 1-D double chain organic–inorganic hybrid Cu–Ln heterometallic GTs $[H_2dap][Cu(dap)_2(H_2O)][Cu(dap)_2]_{0.5}[Ln(H_2O)_3(\alpha\text{-}GeW_{11}O_{39})]\cdot 3H_2O$ [Ln = La^{III} (**1**), Pr^{III} (**2**), Nd^{III} (**3**), Sm^{III} (**4**), Eu^{III} (**5**), Tb^{III} (**6**), Er^{III} (**7**)] under hydrothermal conditions, which are structurally characterized by elemental analyses, IR spectra, PXRD, TG analyses XPS and single-crystal X-ray diffraction. X-ray diffraction structural analyses indicate that **1–7** are isomorphic and adopt novel 1-D double-chain architectures constructed by two antiparallel 1-D polymeric chains linked through $[Cu(dap)_2]^{2+}$ linkages. As far as we know, they exemplify a scare type of organic–inorganic hybrid 1-D double chain Cu–Ln heterometallic GTs. The magnetic properties of **2**, **4** and **7** have been measured and their magnetic behaviors are mainly affected by Ln centers with strong spin–orbit coupling contribution and /or the ligand-field perturbation. The TG curves of **2**, **5**, **6** and **7** show two steps of weight loss between 25 and 700 °C. Furthermore, the solid-state electrochemical and electro-catalytic properties of **3** and **4** have been evaluated. The electrocatalytic reductions of hydrogen

peroxide and bromate are principally mediated by the W^{VI}-based wave while the reduction of nitrite is simutaneously mediated by the W^{VI}-based wave and Cu^{II}-based wave. In short, **3**-CPE and **4**-CPE have obvious electro-catalytic activities for the reductions of hydrogen peroxide, bromate and nitrite. The key points of the synthetic procedures have been well established. In the future, other functional organic ligands such as aliphatic polycarboxylic acid, aromatic polycarboxylic acid and amino acid ligands will be introduced to this system to made TM–Ln cluster substituted GTs with novel architectures and excellent functional properties. It can be believed that these findings are very significant in exploring the syntheses of organic–inorganic hybrid TM–Ln heterometallic GTs, even for PBTLHDs.

Acknowledgements

This work was supported by the Natural Science Foundation of China (21101055, 21301049, U1304208), China Postdoctoral Science Foundation Funded Project (201104392, 20100470996), the Natural Science Foundation of Henan Province (122300410106, 102300410093), the Foundation of State Key Laboratory of Structural Chemistry (20120013), 2012 Young Backbone Teachers Foundation from Henan Province and the 2012, 2013 Students Innovative Pilot Plans of Henan University.

References

[a] *Institute of Molecular and Crystal Engineering, Henan Key Laboratory of Polyoxometalate Chemistry, College of Chemistry and Chemical Engineering, Henan University, Kaifeng, Henan 475004, P. R. China. Email: zhaojunwei@henu.edu.cn*

[b] *State Key Laboratory of Structural Chemistry, Fujian Institute of Research on the Structure of Matter, Chinese Academy of Sciences, Fuzhou, Fujian 350002, P. R. China. Email: ygy@fjirsm.ac.cn*

† Electronic Supplementary Information (ESI) available: The refinement details, bond valence sum calculations, additional figures and thermogravimetri analyses. CCDC reference numbers 967042–967048 for **1**–**7**. For ESI and crystallographic data in CIF or other electronic format see DOI: 10.1039/ b000000x/

1 (*a*) M. T. Pope, *Heteropoly and Isopoly Oxometalates.* Springer-Verlag, Berlin. Germany, **1983**; (*b*) J. J. Borras-Almenar, E. Coronado, A. Müller and M. T. Pope, *Polyoxometalate Molecular Science*. Kluwer Academic Publishers, Dordrecht, The Netherlands, **2003**; (*c*) M. AlDamen, J. Clemente-Juan, E. Coronado, C. Martí-Gastaldo and A. Gaita-Ariño, *J. Am. Chem. Soc.*, 2008, **130**, 8847; (*d*) C. Ritchie, A. Ferguson, H. Nojiri, H. N. Miras, Y. F. Song, D. L. Long, E. Burkholder, M. Murrie, P. Kögerler, E. Brechin and L. Cronin, *Angew. Chem. Int. Ed.*, 2008, **47**, 5609; (*e*) A. Dolbecq, E. Dumas, L. C. Francescoin and M. R. Antonio, *Inorg. Chem.*, 2008, **47**, 6889.

2 (*a*) B. Godin, Y. Chen, J. Vaissermann, L. Ruhlmann, M. Verdaguer and P. Gouzerh, *Angew. Chem. Int. Ed.*, 2005, **44**, 3072; (*b*) S. S. Mal and U. Kortz, *Angew. Chem. Int. Ed.*, 2005, **44**, 3777; (*c*) G. S. Kim, H. D. Zeng, D. Van Derveer and C. L. Hill, *Angew. Chem. Int. Ed.*, 1999, **38**, 3205; (*d*) Y. Sakai, K. Yoza, C. N. Kato and K. Nomiya, *Chem. Eur. J.*, 2003, **9**, 4077; (*e*) S. T. Zheng, J. Zhang, J. M. Clemente-Juan, D. Q. Yuan and G. Y. Yang, *Angew. Chem. Int. Ed.*, 2009, **48**, 7176; (*f*) B. S. Bassil, M. Ibrahim, R. Al-Oweini, M. Asano, Z. Wang, J. van Tol, N. S. Dalal, K. Y. Choi, R. N. Biboum, B. Keita, L. Nadjo and U. Kortz, *Angew. Chem. Int. Ed.*, 2011, **50**, 5961; (*g*) P. I. Molina, H. N. Miras, D. L. Long and L. Cronin, *Inorg. Chem.*, 2013, **52**, 9284.

3 (*a*) T. Yamase, *Chem. Rev.*, 1998, **98**, 307; (*b*) C. Benelli and D Gatteschi, *Chem. Rev.*, 2002, **102**, 2369; (*c*) H. E. Moll, B. Nohra, P. Mialane, J. Marrot, N. Dupré, B. Riflade, M. Malacria, S. Thorimbek, B. Hasenknopf, E. Lacôtc, P. A. Aparicio, X. López, J. M. Poblet and A. Dolbecq, *Chem. Eur. J.*, 2011, **17**, 14129; (*d*) Y. Kikukawa, S. Yamaguchi, K. Tsuchida, Y. Nakagawa, K. Uehara, K. Yomaguchi and N. Mizuho, *J. Am. Chem. Soc.*, 2008, **130**, 5472; (*e*) C. Boglio, B. Lemiére, Hasenknopf, S. Thorimbert, E. Lacôte and M. Malacria, *Angew. Chem. Int. Ed.*, 2006, **45**, 3324.

4 (*a*) K. Wassermann, M. H. Dickman and M. T. Pope, *Angew. Chem. Int. Ed.*, 1997, **36**, 1445; (*b*) R. C. Howell, F. G. Perez, S. Jain, Jr. W. D. Horrocks, A. L. Rheingold and L. C. Francesconi, *Angew. Chem. Int. Ed.*, 2001, **40**, 4031; (*c*) G. L. Xue, J. Vaissermann and P. Gouzerh, *J. Cluster Sci.*, 2002, **13**, 409; (*d*) K. Fukaya and T. Yamase, *Angew. Chem. Int. Ed.*, 2003, **42**, 654; (*e*) B. S. Bassil, M. H. Dickman, I. Römer, B. von der Kammer and U. Kortz, *Angew. Chem. Int. Ed.*, 2007, **46**, 6192.

5 H. Y. An, Y. Lan, Y. G. Li, E. B. Wang, N. Hao, D. R. Xiao, L. Y. Duan and L. Xu, *Inorg. Chem. Commun*., 2004, **7**, 356.

6 (*a*) J. D. Compain, P. Mialane, A. Dolbecq, I. M. Mbomekallé, J. Marrot, F. Sécheresse, Duboc, C.; E. Rivière. *Inorg. Chem.*, 2010, **49**, 2851; (*b*) X. J. Feng, W. Z. Zhou, Y. G. Li, H. S. Ke, J. K. Tang, R. Clérac, Y. H. Wang, Z. M. Su and E. B. Wang, *Inorg. Chem*., 2012, **51**, 2722; (*c*) D. Y. Shi, J. W. Zhao, L. J. Chen, P. T. Ma, J. P. Wang, and J. Y. Niu, *CrystEngComm*, 2012, **14**, 3108.

7 (*a*) C. D. Wu, C. Z. Lu, H. H. Zhuang and J. S. Huang, *J. Am. Chem. Soc.*, 2002, **124**, 3836; (*b*) P. Mialane, A. Dolbecq, E. Riviére, J. Marrot and F. Sécheresse, *Eur. J. Inorg. Chem.*, 2004, 33.

8 S. Reinoso, *Dalton Trans*., 2011, **40**, 6610.

9 (*a*) W. L. Chen, Y. G. Li, Y. H. Wang and E. B. Wang, *Eur. J. Inorg. Chem.*, 2007, 2216; (*b*) X. K. Fang and P. Kögerler, *Angew. Chem., Int. Ed.*, 2008, **47**, 8123; (*c*) X. K. Fang and P. Kögerler, *Chem. Commun.*, 2008, 3396; (*d*) W. L. Chen, Y. G. Li, Y. G. Wang, E. B. Wang and Z. M. Zhang, *Dalton Trans.*, 2008, 865; (*e*) J. F. Cao, S. X. Liu, R. G. Cao, L. H. Xie, Y. H. Ren, C. Y. Gao and L. Xu, *Dalton Trans.*, 2008, 115; (*f*) B. Nohra, P. Mialane, A. Dolbecq, E. Rivière, J. Marrot and F. Sécheresse, *Chem. Commun.*, 2009, 2703; (*g*) Y. W. Li, Y. G. Li, Y. H. Wang, X. J. Feng, Y. Lu and E. B. Wang, *Inorg. Chem.*, 2009, **48**, 6452; (*h*) D. Y. Du, J. S. Qin, S. L. Li, Y. Q. Lan, X. L. Wang and Z. M. Su, *Aust. J. Chem.*, 2010, **63**, 1389; (*i*) S. Yao, Z. M. Zhang, Y. G. Li, Y. Lu, E. B. Wang and Z. M. Su, *Cryst. Growth Des.*, 2010, **10**, 135; (*j*) J. Y. Niu, S. W. Zhang, H. N. Chen, J. W. Zhao, P. T. Ma and J. P. Wang, *Cryst. Growth Des.*, 2011, **11**, 3769; (*k*) Z. M. Zhang, Y. G. Li, S. Yao and E. B. Wang, *Dalton Trans.*, 2011, **40**, 6475; *(l)* S. W. Zhang, J. W. Zhao, P. T. Ma, J. Y. Niu and J. P. Wang, *Chem. Asian J.*, 2012, **7**, 966; (*m*) A. H. Ismail, B. S. Bassil, G. H. Yassin, B. Keita and U. Kortz, *Chem. Eur. J.*, 2012, **18**, 6163; (*n*) H. Y. Zhao, J. W. Zhao, B. F. Yang, H. He and G. Y. Yang, *CrystEngComm*, 2013, **15**, 5209; (*o*) H. H. Wu, S. Yao, Z. M. Zhang, Y.G. Li, Y. Song, Z. J. Liu, X. B. Han and E. B. Wang, *Dalton Trans.*, 2013, **42**, 342.

10 (*a*) S. Reinoso and J. R. Galán-Mascarós, *Inorg. Chem.*,2010, **49**, 377; (*b*) S. Reinoso, J. R. Galán-Mascarós and L. Lezama, *Inorg. Chem.*, 2011, **50**, 9587; (*c*) S. Reinoso, M. Giménez-Marqués, J. R. Galán-Mascarós, P. Vitoria and J. M. Gutiérrez- Zorrilla, *Angew. Chem. Int. Ed.*, 2010, **49**, 8384.

11 U. Kortz, S. Nellutla, A. C. Stowe, N. S. Dalal, U. Rauwald, W. Danquah and D. Ravot, *Inorg. Chem.*, 2004, **43**, 2308.

12 (*a*) J. W. Zhao, D. Y. Shi, L. J. Chen, Y. Z. Li, P. T. Ma, J. P. Wang and J. Y. Niu, *Dalton Trans.* 2012, **41**, 10740; (*b*) J. W. Zhao, D. Y. Shi, L. J. Chen, P. T. Ma, J. P. Wang, J. Zhang and J. Y. Niu, *Cryst. Growth Des.*, 2013, **13**, 4368.

13 L. H. Bi, U. Kortz, S. Nellutla, A. C. Stowe, van J. Tol, N. S. Dalal, B. Keita and L. Nadjo, *Inorg. Chem.*, 2005, **44**, 896.

14 (*a*) G. M. Sheldrick, *SHELXS 97, Program for Crystal Structure Solution*, University of Göttingen, Göttingen, Germany, **1997**; (*b*) G. M. Sheldrick, *SHELXL 97, Program for Crystal Structure Refinement*, University of Göttingen, Germany, **1997**.

15 (*a*) W. J. Niu, D. Y. Shi, J. W. Zhao, X. M. Cai and L. J. Chen, *Inorg. Chem.Commun.*, 2012, **17**, 79; (*b*) L. J. Chen, D. Y. Shi, J. W. Zhao, Y. L. Wang, P. T. Ma and J. Y. Niu, *Inorg. Chem. Commun.*, 2011, **14**, 1052.

16 (*a*) B. Li, J. W. Zhao, S. T. Zheng and G. Y. Yang, *J. Clust. Sci.*, 2009, **20**, 503; (*b*) N. Haraguchi, Y. Okaue, T. Isobe and Y. Matsuda, *Inorg. Chem.*, 1994, **33**, 1015.

17 (*a*) I. D. Brown and D. Altermatt, *Acta Cryst.*, 1985, **B41**, 244; (*b*) A. Trzesowska, R. Kruszynski and J. T. Bartczak, *Acta. Cryst.*, 2004, **B60**, 174; (*c*) N. E. Brese and M. O. Keeffe, *Acta. Cryst.*, 1991, **B47**, 192.

18 (*a*) H. Martinez, A. Benayad, D. Gonbeau, P. Vinatier, B. Pecquenard and *A.* Levasseur, *Appl. Surf. Sci.*, 2004, **236**, 377; (*b*) I. M. Szilágyi, F. Hange, J. Madarász and G. Pokol, *Eur. J. Inorg. Chem.*, 2006, 3413; (*c*) O. Y. Khyzhuna, T. Strunskusb, S. Crammc, Y. M. Solonina, *J. Alloys Compd.*, 2005, **389**, 14; (*d*) K. Yu, Y. G. Li, B. B. Zhou, Z. H. Su, Z. F. Zhao and Y. N. Zhang, *Eur. J. Inorg. Chem.*, 2007, 5662; (*e*) V. B. Kumar, R. Velchuri, V. R. Devi, B. Sreedhar, G. Prasad, D. J. Prakash, M. Kanagaraj, S. Arumugam and M. Vithal, *J. Solid State Chem.*, 2011, **184**, 264; (*f*) T. Akitsu and Y. Einaga, *Polyhedron*, 2006, **25**, 2655; (*g*) R. Vercaemst, D. Poelman, L. Fiermans, R. L. Meirhaeghe, Van, W. H. Laflère and F. Cardon, *J. Electron Spectrosc. Relat. Phenom.*, 1995, **74**, 45.

19 (*a*) B. Li, J. W. Zhao, S. T. Zhen and G. Y. Yang, *Inorg. Chem.*, 2009, **48**, 8294; (*b*) B. Bassil, S. Nellulta, U. Kortz, A. C. Stowe, van J. Tol, N. S. Dala, B. Keita and L. Nadjio, *Inorg. Chem.*, 2005, **44**, 2659.

20 (*a*) M. Sadakane, M. H. Dickman and M. T. Pope, *Angew. Chem. Int. Ed.*, 2000, **39**, 2914; (*b*) P. Mialane, L. Lisnard, A. Mallard, J. Marrot, E. Antic-Fidancev, P. Aschehoug, D. Vivien and F. Sécheresse, *Inorg. Chem*., 2003, **42**, 2102; (*c*) J. Y. Niu, J. W. Zhao and J. P. Wang, *Inorg. Chem. Commun.*, 2004, **7**, 876; (*d*) J. P. Wang, X. Y. Duan, X. D. Du and J. Y. Niu, *Cryst. Growth Des*., 2006, **6**, 2266; (*e*) J. P. Wang, J. W. Zhao, X. Y. Duan and J. Y. Niu, *Cryst. Growth Des*., 2006, **6**, 507; (*f*) J. D. Compain, P. Mialane, A. Dolbecq, I. M. Mbomekallé, J. Marrot, F. Sécheresse, C. Duboc and E. Rivière, *Inorg. Chem.*, 2010, **49**, 2851.

21 (*a*) O. M. Yaghi, M. O'Keeffe, N. W. Ockwig, H. K. Chae, M. Eddaoudi and J. Kim, *Nature*, 2003, **423**, 705; (*b*) B. Moulton and M. J. Zaworotko, *Chem. Rev*., 2001, **101**, 1629.

22 (*a*) E. Coronado and C. J. Gómez-García, *Chem. Rev.*, 1998, **98**, 273; (*b*) P. Q. Zheng, Y. P. Ren, L.S. Long, R. B. Huang and L.S. Zheng, *Inorg. Chem.*, 2005, **44**, 1190; (*c*) J. W Zhao,. S. T. Zheng and G. Y. Yang, *J. Solid State Chem.*, 2008, **181**, 2205.

23 (*a*) O. Kahn, *Molecular Magnetism;* VCH: Weinheim, 1993; (*b*) S. Wang, Z. Pang, K. D. L. Smith and M. J. Wanger, *J. Chem. Soc. Dalton Trans.*, 1994, 955; (*c*) O. Kahn, Adv. *Inorg. Chem.*, 1995, **43**, 179; (*d*) A. C. Rizzi, R. Calvo, R. Baggio, M. T. Garland, O. Peña and M. Perec, *Inorg. Chem.*, 2002, **41**, 5609.

24 (*a*) M. L. Kahn, J. Sutter, S. Golhen, P. Cuionneau, L. Ouahab, O. Kahn and D. Chasseau, *J. Am. Chem. Soc*., 2000, **122**, 3413; (*b*) Y. Q. Sun, J. Zhang, Y. M. Chen and G. Y. Yang, *Angew. Chem. Int. Ed.*, 2005, **44**, 5814; (*c*) S. W. Zhang, Y. Wang, J. W. Zhao, P. T. Ma, J. P. Wang and J. Y. Niu, *Dalton Trans.*, 2012, **41**, 3764.

25 (*a*) C. Benelli and D. Gatteschi, *Chem. Rev.*, 2002, **102**, 2369; (*b*) T. Peristeraki, M. Samios, M. Siczek, T. Lis and C. J. Milios, *Inorg. Chem*., 2011, **50**, 5175; (*c*) Y. Li, F. K. Zheng, X. Liu, W. Q. Zou, G. C. Guo, C. Z. Lu and J. S. Huang, *Inorg. Chem.*, 2006, **45**, 6308; (*d*) J. K. Tang, Y. Z. Li, Q. L. Wang, E. Q. Gao, D. Z. Liao, Z. H. Jiang, S. P. Yan, P. Cheng, L. F. Wang and G. L. Wang, *Inorg. Chem.*, 2002, **41**, 2188; (*e*) T. Arumuganathan and S. K. Das, *Inorg. Chem.*, 2009, **48**, 496; (*f*) M. Andruh, E. Bakalbassis, O. Kahn, J. C. Trombe, P. Porcher, *Inorg. Chem.*, 1993, **32**, 1616; (*g*) J. Y. Niu, K. H. Wang, H. N. Chen, J. W. Zhao, P. T. Ma, J. P. Wang, M. X. Li, Y. Bai, D. B. Dang, *Cryst. Growth Des.*, 2009, **9**, 4362; (*h*) M. L. Kahn, R. Ballou, P. Porcher, O. Kahn and J. P. Sutter, *Chem. Eur. J.*, 2002, **8**, 525; (*i*) A. Caneschi, A. Dei, D. Gatteschi, S. Poussereau and L. Sorace, *Dalton Trans.*, 2004, 1048; (*j*) X. Feng, J. S. Zhao, B. Liu, L. Y. Wang, S. Ng, G. Zhang, J. G. Wang, X. G. Shi and Y. Y. Liu, *Cryst. Growth. Des.*, 2010, **10**, 1399; (*k*) Z. H. Zhang, Y. Song, T. A. Okamura, Y. Hasegawa, W. Y. Sun and N. Uwyama, *Inorg. Chem.*, 2006, **45**, 2896.

26 (*a*) J. E. Toth and F. C. Anson, *J. Am. Chem. Soc.*, 1989, **111**, 2444; (*b*) X. L. Wang, Z. H. Kang, E. B. Wang and C. W. Hu, *Mater. Lett.*, 2002, **56**, 393; (*c*) Z. Zhang, Y. Qi, C. Qin, Y. Li, E. Wang, X. Wang, Z. Su and L. Xu, *Inorg. Chem.*, 2007, **46**, 8162.

27 (*a*) S. Dong, X. Xi and M. Tian, *J. Electroanal. Chem*., 1995, **385**, 227; (*b*) J. E. Toth and F. C. Anson, *J. Electroanal. Chem*., 1988, **256**, 361.

28 (*a*) J. Wang, Y. Lin and L. Chen, *Analyst.*, 1993, **118**, 277;. (*b*) X. L. Wang, H. Zhang, E. B. Wang, Z. B. Han and C. W. Hu, *Mater. Lett.*, 2004, **58**, 1661; (*c*) Z. F. Li, J. H. Chen, D. W. Pan, W. Y. Tao, L. H. Nie and S. Z. Yao, *Electrochim. Acta.*, 2006, **51**, 4255; (*d*) H. J. Pang, J. Peng, J. Q. Sha, A. X. Tian, P. P. Zhang, Y. Chen and M. Zhu, *J. Mol. Struct.* 2009, **921**, 289; (*e*) B. Keita, P. de Oliveira, L. Nadjo and U. Kortz, *Chem. Eur. J.*, 2007, **13**, 5480; (*f*) X. Wang, H. Hu, A. Tian, H. Lin and J. Li, *Inorg. Chem.*, 2010, **49**, 10299.

Syntheses, structures and electrochemical properties of a class of 1-D double chain polyoxotungstate hybrids $[H_2dap][Cu(dap)_2]_{0.5}[Cu(dap)_2(H_2O)][Ln(H_2O)_3(\alpha\text{-}GeW_{11}O_{39})]\cdot 3H_2O$

Jun-Wei Zhao,* Yan-Zhou Li, Fan Ji, Jing Yuan, Li-Juan Chen and Guo-Yu Yang*

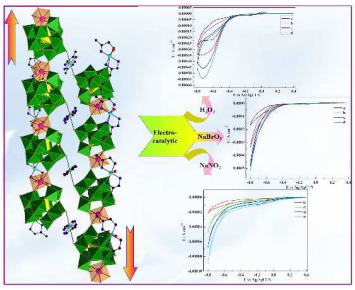

A series of novel organic–inorganic hybrid 1-D double chain germanotungstates **1**–**7** are the first 1-D double-chain Cu^{II}–Ln^{III} heterometallic germanotungstates.